Separation & Purification Reviews
Publication details, including instructions for authors and subscription information:
http://www.informaworld.com/smpp/title~content=t713597294

Reverse Osmosis Separations With Aromatic Polyamide Films and Hollow Fibers

R. McKinney Jr.[a]
[a] Chemstrand Research Center, Inc., Durham, North Carolina

To cite this Article McKinney Jr., R.(1973) 'Reverse Osmosis Separations With Aromatic Polyamide Films and Hollow Fibers', Separation & Purification Reviews, 1: 1, 31 — 115
To link to this Article: DOI: 10.1080/03602547308068938
URL: http://dx.doi.org/10.1080/03602547308068938

REVERSE OSMOSIS SEPARATIONS WITH AROMATIC POLYAMIDE FILMS AND HOLLOW FIBERS

R. McKinney, Jr.
Chemstrand Research Center, Inc.
Durham, North Carolina 27702

I. INTRODUCTION

Reverse osmosis as a means of separation and purification has grown from little more than a laboratory curiosity to a commercial process in less than two decades, the impetus for such technological progress having been supplied almost entirely by the Office of Saline Water of the U. S. Department of the Interior.

The events which initiated this technological growth first occurred with the discovery by Reid[1] of cellulose acetate as an effective membrane material, together with the subsequent demonstration by Loeb and Sourirajan[2,3] that high-flux cellulose acetate membranes could be produced. During the ensuing years, the bulk of successful membrane development has been limited to the adaptation of cellulose esters in general, and cellulose acetate in particular, to brackish and seawater demineralization.

In this chapter, the reverse osmosis performance of a novel membrane system based on a class of aromatic polyamide and polyamide-hydrazide polymers, first observed[4,5,6] by the author in 1968 and independently by Richter et al.,[7] is described.

So unique are the combined transport and mechanical properties of the membranes prepared from these polymers that, in time, it is the author's view they may well supplant cellulose acetate as the dominant membrane composition for separation and purification applications.

II. MEMBRANE PREPARATION

A. Polymer Synthesis

The aromatic polyamide and polyamide-hydrazide polymers were prepared by low-temperature solution polymerization in dimethylacetamide (DMAc). The aromatic polyamide polycondensation reactions were carried out in the temperature range: $-20 \leq t, ^\circ C \leq -10$ utilizing isophthaloyl and terephthaloyl chloride as the acid-chlorides and 1,3-bis(3-aminobenzamide)-benzene, 3,4'-diaminobenzanilide, m-phenylene diamine, and 3,5'-diaminobenzoic acid as the diamines.

The synthesis of the aromatic polyamide-hydrazides was carried out in the temperature range: $-10 \leq t, ^\circ C \leq +5$ again,

using isophthaloyl and terephthaloyl chloride as the acid-chlorides, and meta and paraaminobenzhydrazide as the amine-hydrazide. The structural formulas for the repeat units of these polymers are given in Figure 1.

At the conclusion of the polymerization reaction, calcium carbonate, in quantities sufficient to neutralize 95 mol % of the HCl liberated during the polycondensation reaction, was stirred into the polymer solution. The mixture was heated to 75-80° C to achieve complete reaction of the $CaCO_3$ and then vacuum degassed. By this procedure, polymer molecular weights in the range: $20 \leq 10^{-3} \bar{M}_v \leq 70$ were attained. The solutions were then filtered through a 5-micron pore-size filter and used directly for the preparation of asymmetric membranes. The same procedure was employed in dope preparation for homogenous membrane production, except that the neutralization step was omitted.

B. Membrane Formation

1. Asymmetric Membranes

The preparation of asymmetric, aromatic polyamide membranes consists of three basic stages: casting the membrane to a uniformly controlled thickness; evaporating a portion of the solvent at a rate sufficient to establish a solvent concentration

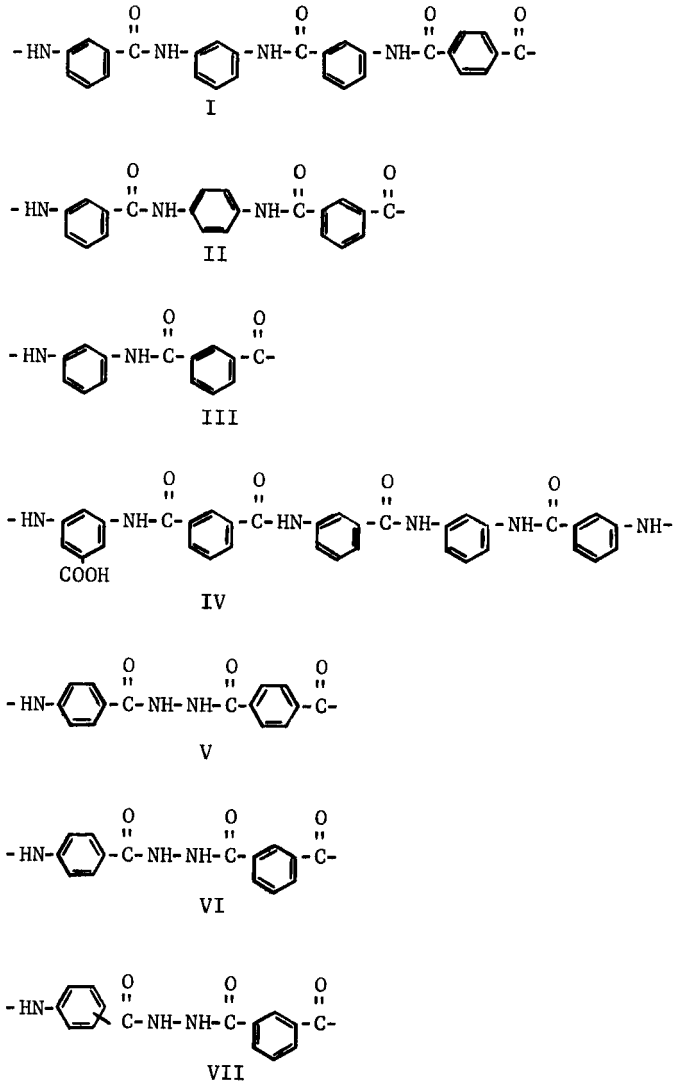

FIGURE 1

Structural Units of the Aromatic Polyamides and Polyamide-Hydrazides

gradient; and, finally, fixing or preserving this compositional gradient by coagulation in water.

During the solvent evaporative period, two important processes occur simultaneously: skin formation (a stratum densification in the film at the film/air interface) and an overall decrease in the level of solvent in the cast solution. Hansen[8,9] has shown that the solvent loss rate, for a drying polymer film on an impermeable substrate, is dependant upon two barriers. The first barrier is dominant at the air-solution interface and is the consequence of such factors as vapor pressure and the latent heat of vaporization of the solvent; while the second barrier resides within the cast film and is the result of a diffusion-limited process. Both barriers are significant parameters in membrane formation, controlling the level of solvent in the drying solution and, hence, in the final membrane structure. Under coagulation conditions of a given solvent/non-solvent pair, at constant temperature, the pore structure and matrix density of an asymmetric membrane will be dependant upon the level of solvent in the drying film at the time of coagulation. High solvent levels generally give a more open matrix structure while, in the extreme case, a completely dry film would show no coagulation effects, as evidenced by a complete lack of porosity.

During coagulation, two simultaneous processes occur at the membrane-coagulant interface: diffusion of non-solvent into and solvent out of the membrane solution. The driving forces for these processes are the chemical potential gradients established across the membrane skin for both the solvent and non-solvent (coagulant) components.

As the non-solvent diffuses into the membrane gel it becomes diluted with the solvent and its effectiveness as a coagulant diminishes temporarily. As more non-solvent diffuses across the membrane skin the activity for this component in the membrane phase increases, thereby reducing its driving potential and hence its diffusion rate. Simultaneously the solvent diffuses out of the membrane without any corresponding activity change, due to its dilution in the comparatively enormous volume of the non-solvent. Thus, its diffusion rate is essentially unaltered. Because of the negative coagulant rate change, the diffusion rate ratio of solvent to non-solvent increases, enhancing solvent loss over coagulation and thereby aiding the formation of a denser membrane structure. If the solvent system used in preparing the membranes is a thermodynamically good solvent (high cohesive energy density) and capable of tolerating large quantities of water, the normal coagulant used in membrane preparation, then the

matrix density of the membrane will be even greater, especially at the casting support surface--the last region to see the coagulant. For example, our studies have shown the DMAc/$CaCl_2$ solvent system capable of tolerating weight percent water levels equal to that for the polymer in solution before any evidence of phase change (precipitation) appears. Therefore it is reasonable to conclude that very large amounts of non-solvent (water), provided by very low solvent/non-solvent diffusion rate ratios, are necessary for effective coagulation of this system. Removal of the coagulating membrane from its impermeable substrate (glass plate) would, in principal, increase the rate of coagulation. However, the coagulant must first reach this surface in order to provide the necessary matrix metastasis for release from the glass plate. Indeed, such release would be evidence of rapid coagulation. Mechanical means for membrane removal might be employed, but always at the risk of damage to the very thin and comparatively fragile skin.

The membranes described in this chapter were prepared from carefully filtered polymer solutions, previously described, by casting at a uniform thickness (ca. 0.05 cm) on a glass plate using a Gardner(R) knife with adjustable blade. The cast film was then placed in an oven equipped with a filtered air intake. The

cast solutions were dried at temperatures in the range: $80 \leq t$, $^{\circ} C \leq 120$ for periods up to 240 minutes, followed by coagulation in distilled or deionized water.

A similar procedure is utilized in the preparation of asymmetric aromatic polyamide-hydrazide membranes with one exception. An additional post-treatment step, similar to that employed for cellulose acetate, is required to achieve high selectivity to dissolved salts. Such treatment involves the brief exposure of the membrane to water at an elevated temperature in order to consolidate the skin or layer previously established during the oven drying period.

2. Homogeneous Membranes

Homegeneous membranes are those in which the cross-sectional density is isotropic. To obtain this kind of structural homogeneity in the aromatic polyamide and polyamide-hydrazide membranes for use in basic transport studies, solutions free of any non-volatile, and leachable components, must be employed. Otherwise porosity will be introduced as the component is extracted. To achieve this desired structure, unneutralized or acid dopes (containing only polymer, dimethylacetamide and hydrochloric acid) are utilized. The HCl is vaporized along with the solvent during drying.

Because of the lack of salt in the unneutralized solutions, some care must be exercised in the selection of membrane drying temperatures, owing to the inverse solubility-temperature relationship for these polymers in dimethylacetamide. Phase separation is evident in membranes prepared from unneutralized dopes at temperatures above ca. 80° C. Such morphological changes will result in considerable void fraction in the final membrane.

C. Membrane Evaluation

Reverse osmosis measurements with flat membranes were carried out with a membrane tester previously described.[10] The addition of a high pressure diaphragm pump facilitated testing over extended periods. To reduce corrosion and subsequent membrane fouling, long-term (≥ one month) laboratory tests were carried out in a test unit (Figure 2) constructed entirely from polyvinyl chloride, except for the pressure gauge isolation unit, which was constructed from Inconel 625, and the pump, which had type 316 stainless steel connection ports.

Membrane defects were determined, prior to reverse osmosis testing, in the following manner. The membrane was loaded into the test cell and the unit was bolted with the recommended torque. A small volume (ca. 5 ml) of an aqueous crystal

FIGURE 2
PVC Reverse Osmosis Test Unit

violet dye solution was injected into the cell above the membrane and the unit was pressurized (to about 7 atms). Evidence of any

dye in the product-side solution was indicative of a significant defect and, in these cases, the membranes were discarded.

For membranes judged defect-free at this point, the dye solution was washed from the cell and the reverse osmosis tests begun. This dye procedure was duplicated at the conclusion of the tests, the cell was disassembled, and the membrane was examined for dye spots. The selective or active side of these membranes will not accept this dye; however, the matrix side will, and thus staining indicates a discontinuity in the skin.

The standard reverse osmosis test procedures used in evaluating the membranes described in this chapter were: sodium chloride concentrations/pressures of: 0.08M/41 atms and 0.6M and 1.03M at 102 atms. All tests with natural seawater were conducted at pressures of 102 atms.

III. PROPERTIES OF AROMATIC POLYAMIDE MEMBRANES

A. Transport Data

The solution-diffusion model for membrane transport, including a special case allowing for membrane imperfections, has been generally accepted as an adequate mathematical description of the transport processes occurring in uncharged membranes operating under conditions of reverse osmosis.

This model has been exhaustively described[11,12,13] and will be mentioned here only for the sake of clarity and continuity.

The two basic assumptions of this model are that Fick's law is obeyed and that uncoupled flow occurs (the flow of one component is unaffected by the flow of other components within the membrane). It is further assumed that adequate boundary conditions are maintained, i.e. the chemical potential is continuous across the membrane-solution interface. Each species then permeates the membrane under the influence of its chemical potential gradient, determined by the concentration and pressure gradients.

For the solvent component, it can be shown that the flux (J_1) is given by

$$J_1 = \frac{D_1 C_1 \bar{V}_1}{RT\lambda} (\Delta P - \Delta\pi) \qquad (1)$$

where the quantities D_1, C_1, and $\bar{V}_1$ are the solvent diffusion coefficient, solvent concentration in the membrane, and the partial molar volume (of water); R and T are the gas constant and absolute temperature; λ the effective membrane thickness (the skin thickness for an asymmetric membrane, provided that the matrix offers no flow resistance, and the entire thickness of a truly homogeneous membrane); and $(\Delta P - \Delta\pi)$ the net driving

pressure obtained by the difference between the applied (P) and osmotic (π) pressures, respectively.

For the solute, the flux (J_2) is given by

$$J_2 = -\frac{D_2 K}{\lambda} (\Delta C_2) \qquad (2)$$

in which D_2 is the diffusion coefficient for the solute, K its distribution coefficient (g/cm^3 of solute in the membrane divided by the g/cm^3 of solute in the surrounding solution), and ΔC_2 the solute concentration gradient across the membrane.

The solute rejection (r) is given by[11]

$$r = \left[1 + \frac{D_2 K R T C_1^*}{D_1 C_1 \bar{V}_1 (\Delta P - \Delta \pi)}\right]^{-1} \qquad (3)$$

where C_1^* is the concentration of water in solution on the low pressure side of the membrane. For membranes of high rejection, the value of unity is usually assigned to this term.

Substituting water-transport data into Eq. (1), one can calculate a water permeability coefficient defined by $P_1 = D_1 C_1$. With knowledge of ΔC_2 and J_2, one can then calculate a salt permeability coefficient given to be: $P_2 = D_2 K$. With such data, available from homogeneous membrane studies, one is now able to predict the performance (flux and rejection) of a membrane of anisotropic structure having a skin of preassigned thickness.

In making such performance extrapolations, two assumptions are mandatory. First, the homogeneous or dense membrane must be of uniform cross-sectional density. Secondly, and equally important, the density of the homogeneous membrane must correspond to that present in the skin or active layer of the asymmetric membrane. Generally speaking, the latter condition is readily met when working with essentially amorphous polymers such as 39.8% acetyl cellulose acetate, since a constant morphology can be expected over rather wide variations in preparative conditions. Data from crystalline or potentially crystalline polymers, on the other hand, must be examined with some caution since small alterations in preparative conditions (drying temperature and time, solvent composition, etc.) could, in principal, contribute to considerable variation in membrane morphology and subsequent transport behavior making performance comparisons difficult if not impossible. Such consideration was given to the comparisons made with transport data for aromatic polyamide membranes.

1. Homogeneous Membranes

The water and salt permeabilities for selected homogeneous membranes, prepared according to the procedure previously described in this chapter, are summarized in Table I (including

TABLE I

Water and Salt Permeability Data for Selected Homogeneous Aromatic Polyamide Membranes

Polymer	Duration of Oven Exposure (mins.)	Membrane Thickness 10^3(cm)	C_1 (g/cm^3)	J_1 10^6(g/cm^2-sec)	P_1 10^7(g/cm^2-sec)	J_2 10^{10}(g/cm^2-sec)	P_2 10^{11}(cm^2/sec)
I	30	2.03	0.30	1.5	0.76	2.7	0.91
	120	1.52	0.19	0.75	0.28	0.45	0.11
	960	2.79	0.17	0.38	0.26	0.68	0.32
	4080	1.78	0.12	0.34	0.15	1.4	0.43
IA	-	5.59	0.16	0.09	0.13	0.11	0.10
II	4080	1.27	0.13	0.34	0.11	0.62	0.13
Cellulose Acetate (39.8% acetyl content)	-	2.8	0.17	2.7	2.6	53	30

Data taken from reverse osmosis measurements carried out at 23°C and 102 atms. with a 1.03 M NaCl test solution.

Data given for a consolidated asymmetric membrane prepared by air drying in a clamp under tension (IA).

V. Merten, "Desalination by Reverse Osmosis", Chapt. 4, p. 105. The MIT Press, Cambridge, 1966.

comparative data for cellulose acetate). The first four entries represent data taken for Polymer I membranes dried for various intervals of time. A continuous decrease with increased oven exposure is observed for the membrane water level (C_1) and water permeability (P_1). This change could be identified with membrane consolidation as the last traces of solvent begin to disappear during the extended drying process. However, for very long oven exposure times ($\geq$ 960 mins), the salt permeability (P_2) is seen to increase. This suggests the onset of appreciable crystallization within the membrane resulting in localized "molecular" voids as more and more polymer is relocated to participate in crystal growth. Further evidence in support of this hypothesis is available from thermal post-treatment studies with asymmetric membranes prepared from Polymer I. The permeabilities for this type of membrane, after permitting it to air dry in a circular holder with O-ring clamp under tension, are given by the fifth entry of Table I. The use of a holder fixes the diameter of the drying membrane allowing only dimensional changes (consolidation) in the membrane thickness to occur. A substantial decrease in P_2 is observed for this system in comparison to the previous entries of this table. This change may result from membrane crystallization as the plasticizing diluent (water) is removed. The value of P_1 is compara-

tively high, in fact, sufficiently so to provide the necessary flux ratios for an observed rejection of 99.8% to NaCl. When this dehydrated membrane was heated to 200° C for 48 hours (in vacuo) the rejection went to zero while the value of J_1 increased to over 7×10^{-4} g/cm^2-sec. The complete lack of selectivity to NaCl, combined with the very large water-flux increase, is indicative of pore-flow resulting from substantial changes in membrane morphology. The complete absence of any opacity (light scattering) development, on heating, suggests that the voids formed are of dimensions smaller than the wave length of light. The membrane also failed to accept crystal violet dye, indicating that very little amorphous polymer remained. These observations lead one to postulate a structure consisting principally of "crystals and holes."

Recognizing the strong dependence of membrane transport behavior on preparative conditions, one must decide which condition provides the morphology most closely corresponding to that found in the skin or active layer of the high flux, asymmetric aromatic polyamide membranes. Typical performance for an asymmetric Polymer I membrane operating at 102 atms with a 1.03M NaCl solution is 37.8×10^{-5} g/cm^2-sec (8 gal/ft^2-day). Applying the values of P_1 for this polymer (Table I, entries 1-5)

one can calculate membrane skin thicknesses of 813, 300, 278, 160 and 140 Å, respectively. The values of P_1 close to 2.8×10^{-8} g/cm^2-sec provide for a skin thickness (ca. 300 Å) that is in excellent agreement with that observed by transmission electron microscopy discussed in detail later in this chapter.

2. Asymmetric Membranes

Considerable evidence for anisotropic structure in high-flux aromatic polyamide and polyamide hydrazide membranes exists. Such evidence includes an inward curling (skin of membrane outside curl) of the membrane during air drying, directional nature of membrane performance under reverse osmosis conditions[6], selective dyeability (skin or active region will not accept dyes such as crystal violet) and direct observation by electron microscopy.

The transport behavior of the aromatic polyamide membrane shows little dependence on oven drying time beyond about 30 mins, as illustrated by entries for Polymer I membranes in Table II. The rate of solvent loss is initially rapid, until the formation of a skin after about 10-15 minutes retards further loss. (Note increase in selectivity at this point.) Beyond this point the level of solvent remains nearly constant, as does the membrane water content (an index of porosity) and flux.

TABLE II

The Effect of Oven Exposure on
Polymer I Membrane Properties

Oven Exposure (mins.)	Rejection	Residual Solvent at Time of Coagulation (g/g of Original Solution)	Flux 10^4(g/cm^2-sec)	Water Content (g/g of Wet Membrane)
4	0.054	0.80	11.9	0.62
15	0.932	0.55	1.46	-
30	0.997	0.39	2.88	0.59
60	0.995	0.37	2.41	0.58
120	0.996	0.37	2.69	0.57
160	0.996	0.35	2.93	0.56
170	0.996	0.35	3.25	-
180	0.994	0.34	3.92	0.54
195	0.995	0.34	2.55	-
220	0.992	0.33	3.63	-
240	0.995	0.33	3.02	0.53
960	0.998	-	1.93	0.49

All membranes cast 5.08×10^{-2} cm from neutralized solutions followed by oven drying at 105± 0.5°C in a mechanical convection oven for the indicated time, then coagulated at 23°C in deionized water.

Reverse osmosis data taken at 41 atoms with a 0.08 M NaCl test solution.

Residual solvent analysis determined gravimetrically and by a ultraviolet spectrophotometric technique.

Water content is the measured g. of water/g. of wet membrane @ 25°C and 100% relative humidity.

A similar behavior is observed for the polyamide-hydrazides, except that the high levels of selectivity evident for the polyamides is seldom realized without an additional thermal post-treatment step (in water).

Annealing the polyamide-hydrazide membrane, after coagulation and after all residual solvent has been extracted, in water at elevated temperatures results in a reduction in flux at an increase in selectivity to dissolved salts. Both changes became essentially asymptotic with time after approximately 15 minutes for a given annealing temperature. There exists a strong dependence of this steady-state flux and rejection with annealing temperature, as shown for Polymer V in Table III.

The effect of coagulation temperature and selected coagulant types was examined for Polymer I membranes as shown in Table IV.

There appears to be a maxima in both flux and rejection, with coagulation temperature in water, occurring near ambient temperatures. This is in contrast to the behavior observed[6] for the aromatic polyamide-hydrazide such as Polymer V. Acetone yields the lowest flux, suggesting a very low coagulation rate, while methanol repeatedly yielded deleterious effects on membrane selectivity.

TABLE III

The Relationship Between Polymer V Transport Properties and Annealing Temperatures

Annealing Temperature (° C)	Average Water Flux 10^4 (g/cm^2-sec)	Rejection
None	14.2	0.60
70	3.8	0.83
85	2.8	0.95
95	1.9	0.96
100	0.9	0.98

All membranes cast 2.54×10^{-2} cm, oven dried for 50 minutes, at 105° C, then coagulated at 24° C in deionized water. Annealing times of 15 minutes were employed at indicated temperatures.

There exists a relatively strong dependence of water flux on temperature for the aromatic polyamide and polyamide-hydrazide membranes, as shown by the activation energies for water permeation in Table V.

As can be seen from the data in Table V, higher operating temperatures result in increased water flux. Each membrane tested showed a slight increase in salt rejection with temperature, suggesting comparatively little dependence of salt permeability on temperature. There is a limitation on the increase in operating temperature permissible, or even desirable, for the improvement

TABLE IV

The Effects of Coagulation Variants on Asymmetric Polymer I Membrane Transport Performance

Coagulant				
Type	Temperature (° C)	J_1 10^5(g/cm^2-sec)	r	Water Content (g/g of wet membrane)
Water	0	9.91	0.997	0.46
	25	23.1	0.999	0.51
	45	16.5	0.995	0.55
Acetone	25	0.19	0.995	0.39
Methanol	25	8.97	0.428	0.69
Propanol	25	6.14	0.994	0.43
Ethylene glycol:water (50:50)	25	5.19	0.982	0.53

All membranes cast 25.4 x 10^{-3} cm followed by oven drying for 60 minutes at 100° C. Coagulation occurred in deionized water at 23° C.

of membrane flux. Eventually, transitions occur within the membrane on heating, resulting in a decrease rather than increase in flux. For example, a plot of flux versus temperature produces an upward curving line to about 45° C for the polyamides (Polymers I and II) at which point the data points begin to level out and even drop. This abrupt rate change may be the glass transition temperature for these polymers in water. Regardless of the cause, the long-term usefulness of the membrane is diminished considerably.

TABLE V

The Effects of Temperature on Water Flow in Aromatic Polyamide Membranes

Polymer	Performance at 25°C J_1 10^4(g/cm^2-sec)	r	$\frac{dJ_1}{dt}$ (20≤t,° C≤30) (%/° C)	ΔHa (Kcal/mol)
I	3.8	0.995	4.7	7.2
II	4.1	0.990	4.0	6.2
V	0.9	0.946	3.3	4.4
VI	4.1	0.971	3.6	6.0

Membrane reverse osmosis data taken at 41 atms with a 0.08M NaCl test solution.

The polyamide-hydrazides studied show considerably improved flux stability over the straight polyamides at elevated temperatures, as illustrated in Table VI.

TABLE VI

The Effects of Temperature on Membrane Flux Stability

Polymer	Temperature (° C)	$\frac{d \log J_1}{d \log t}$	Test Solution	Pressure (atms)	Rejection
I	65	-0.307	distilled water	81.7	-
V	65	-0.112	distilled water	81.7	-
VI	74	-0.050	0.026M NaCl	47.6	0.955

Polymer VI membrane provided the observed low flux decline (Table VI) for a continuous 10 days of operation.

The effects of pressure on the water flux and sodium chloride rejection for an aromatic polyamide (Polymer I) and a polyamide-hydrazide (Polymer V) are summarized in Table VII. A linear response in flux was observed for both membranes up to pressures of 136 atmospheres, with some increases in selectivity evident.

TABLE VII

The Effects of Pressure on the Reverse Osmosis Performance of Asymmetric Polymer I and V Membranes

Pressure (atms)	Polymer I J_1 10^4(g/cm^2-sec)	Polymer I r	Polymer V 10^4(g/cm^2-sec)	Polymer V r
20.4	0.73	0.992	0.52	0.901
40.8	1.46	0.994	0.94	0.913
68.0	2.45	0.994	1.60	0.930
102	3.59	0.996	2.31	0.940
136	4.53	0.996	3.16	0.941

Test carried out with membrane thermostated at 25 $\pm$ 0.01° C with a 0.08M NaCl feed. Polymer I membrane cast 25.4 x 10^{-3} cm followed by oven drying for 30 minutes at 100° C, Polymer V membrane cast same thickness, dried for 50 minutes at 100° C. Both membranes coagulated at 23° C. Polymer V membrane post-treated in 85° C water for 15 minutes.

Studies carried out to assess the effects of various reagents on the reverse osmosis performance of aromatic polyamide membranes have shown the chemical resistance of these systems to be outstanding, especially with regard to hydrolysis. In one experiment, Polymer I membranes were stored in selected reagents for one week at ambient temperatures (ca. 23 ± 2° C) followed by washing in deionized water and testing in triplicate under reverse osmosis conditions of 41 atms and a 0.08M NaCl feed. The data are summarized in Table VIII.

Some morphological changes in the membrane on exposure to the organic reagents occurred, as evidenced by the reduction in membrane flux. However, no changes in physical appearance could be detected with the reagents. Comparable aqueous mixtures of phenol and pyridine did result in detectable, circumferential membrane shrinkage of 11 and 15 percent, respectively. These membranes were therefore not tested.

The aromatic polyamide and polyamide-hydrazide membranes have demonstrated[5] unique ability to reject a rather broad range of solutes. A comparative listing of some of the solutes examined to date, together with pertinent selectivity data, is given in Table IX.

TABLE VIII

The Effects of Selected Reagents on the
Reverse Osmosis Performance of Asymmetric Polymer I Membranes

Test Reagent		J_1		Membrane	Water Content
Type	Concentration	10^5 (g/cm^2-sec)	r	Thickness 10^3 (cm)	(g/g of Wet Membrane)
None	Control	11.8	0.998	5.59	0.61
H_2SO_4	0.2N	9.4	0.994	5.08	0.56
	1.0N	10.4	0.999	4.83	0.54
HCl	0.2N	9.4	0.996	5.08	0.58
	1.0N	9.4	0.987	5.08	0.56
HNO_3	0.2N	12.3	0.985	4.57	0.56
	1.0N	8.5	0.992	5.59	0.56
CH_3COOH	1.0N	36.3	0.351	5.59	0.54
NaOH	0.2N	16.5	0.981	4.83	0.56
	1.0N	9.4	0.982	6.10	0.61
NH_4OH	1.0N	16.5	0.997	5.84	0.57
Acetone	*	4.4	0.997	4.83	0.59
n-methyl pyrrolidone	*	8.0	0.997	6.35	0.53
dimethyl acetamide	*	6.1	0.998	5.84	0.59
dimethyl sulfoxide	*	6.6	0.997	4.83	0.57
dimethyl formamide	*	5.7	0.999	4.57	0.57

* Volume-volume mixtures of (25:75) test reagent:water were used. Membranes tested at 41 atms. with a 0.08 M NaCl feed.

TABLE IX

The Selectivity of Polymer I and V Membranes to Several Feed Solutions

Test Solution		Polymer I		Polymer V	
Nature	Conc. 10^3 (g/cm^3)	Product 10^6 (g/cm^3)	Rejection	Product 10^6 (g/cm^3)	Rejection
NaCl	5.0	10	0.998	100	0.980
Boron (pH = 3.5)	.067	11	0.836	-	-
(pH = 10.2)	.067	1	0.985	-	-
Urea	18	1500	0.917	-	-
Fructose	2	18	0.991	21	0.989
Coffee	5.8 (tds)	2	0.999	-	-
Orange Juice	-	(See note below)		-	-
Acid Mine Drainage	1.33 (as Fe)	0.3	0.999	28	0.979
Polyethylene Glycol (1000 mw)	10	20	0.998	20	0.998

Boric acid (with HCl) was used to obtain the low pH feed while sodium borate (with NaOH) was used for the high pH tests.

Analysis of both the orange juice feed and permeate for the Polymer I membrane by gas chromatography indicated essentially complete selectivity to all but one component, a low boiler ($50 \leq$ b.p., °C ≤ 70) with 58.5% rejection for this component at a product recovery of 75%.

Acid mine drainage sample obtained from Norton, West Virginia consisted of 13.34×10^{-4} g/cm^3 of Fe at a product recovery of 85 percent.

Polymer I membranes have also demonstrated[14] the ability to separate helium from natural gas mixtures. Separation factors near 3000 have been observed for helium from methane. A summary of data typical of this membrane is given in Table X.

Comparative reverse osmosis data for the aromatic polyamide and polyamide-hydrazide membranes, described in this chapter (see Figure 1), are summarized in Table XI. Typically, the highest sodium chloride rejections occur in membranes prepared from Polymer I and VII while the lowest are observed for Polymer III membranes.

TABLE X

Selectivity of Polymer I Membranes to a Selected Gas Mixture

Gas	Permeability $\frac{cm^3\ (STP)\ cm}{cm^2\text{-}sec\text{-}cm\ Hg}$	Solubility $\frac{cm^3\ (STP)}{cm^3\text{-}cm\ Hg}$	Diffusivity (cm^2/sec)	α_{He}
Helium	1.36×10^{-10}	1.39×10^{-6}	9.73×10^{-5}	-
Methane	$\sim 5 \times 10^{-14}$	-	-	~3000
Nitrogen	$\sim 2 \times 10^{-14}$	-	-	~6000
Oxygen	1.96×10^{-12}	2.12×10^{-5}	9.26×10^{-8}	69
Hydrogen	8.93×10^{-11}	5.23×10^{-6}	1.71×10^{-5}	1.5

The permeability values for methane and nitrogen are at the lower limit of sensitivity of the test apparatus.

TABLE XI

Comparative Reverse Osmosis Data for Asymmetric Aromatic Polyamide and Polyamide Hydrazide Membranes

Polymer	J_1 10^4 (g/cm^2-sec)	J_2 10^8 (g/cm^2-sec)	r
I	5.47	7.66	0.996
II	7.22	25.3	0.990
III	4.39	50.7	0.967
IV	7.13	17.5	0.993
V	2.78	19.5	0.980
VI	4.20	13.2	0.991
VII	3.35	5.86	0.995

Membrane data taken with a 0.6M NaCl test solution at 102 atms.

The effects of ionizing radiation (Co^{60}) on Polymer I and II flat membrane performance have also been examined. Membrane discs were cut, to the size necessary for reverse osmosis testing, then placed in air-free water. These membranes, together with small amounts of deoxygenated water, were sealed in polyethylene bags. All of the vapor space was carefully displaced with water before sealing. The envelopes were then placed in a Gammacell Model 220 and irradiated for the various intervals of time illustrated in Table XII.

TABLE XII

The Effects of Ionizing Radiation on the Reverse Osmosis Performance of Polymers I and II Membranes

Gamma Radiation Dose 10^{-6} (Rads)	Polymer I			Polymer II		
	J_1 10^4 (g/cm^2-sec)	r	$\frac{d \log J_1}{d \log t}$	J_1 10^4 (g/cm^2-sec)	r	$\frac{d \log J_1}{d \log t}$
-	3.57	0.997	-0.119	3.67	0.990	-0.099
0.875	2.76	0.996	-0.061	2.77	0.996	-0.081
1.750	2.62	0.997	-0.080	3.25	0.996	-0.071
2.625	2.53	0.997	-0.065	3.25	0.993	-0.106
8.750	2.36	0.997	-0.034	2.74	0.988	-0.022
11.375	-	-	-	2.55	0.990	-0.036

Irradiation experiments utilized a Gammacell Model 220 with a Co^{60} source with a dose rate of 8.75×10^5 rads/hour. Reverse osmosis tests carried out at 102 atms with a 1.03M NaCl test solution.

Extended reverse osmosis testing has been carried out with the polyamide membranes operating on municipal water and in the field with natural seawater feed solutions.

The tests with municipal water feeds were conducted at city line pressures (ca. 5 atms.) for periods up to 220 days. These data are summarized in Table XIII. Little flux decline was evident for these operating conditions, and an increase was observed for Polymer I and V membranes. A slight decay in selectivity with time was found for the polyamide-hydrazide membrane (Polymer V). All samples rejections were somewhat lower than expected. The low operating pressure was no doubt the primary cause for the observed selectivity.

The seawater field tests were conducted at the Field Test Station operated by the Office of Saline Water at Wrightsville Beach, N. C. All membranes tested had rejections in excess of 99 percent to the dissolved salts present in seawater. Membrane fouling (from both organic and inorganic sources) was severe under most conditions, but particularly bad during the summer months, no doubt the result of increased biological and chemical activity. Fouling made membrane flux data particularly difficult to analyze, requiring periodic cleaning with citric acid or other iron solubilizers in order to maintain reasonable levels of flux.

TABLE XIII

Long-term Reverse Osmosis Data for Aromatic Polyamide Membranes on Municipal Water Feeds

Elapsed Time (days)	Polymer I		Polymer II		Polymer V	
	J_1 10^5 (g/cm^2-sec)	r	J_1 10^5 (g/cm^2-sec)	r	J_1 10^5 (g/cm^2-sec)	r
2	3.2	0.926	5.2	0.946	1.5	0.855
4	3.1	0.941	8.5	0.949	1.5	0.855
8	3.5	0.949	5.7	0.956	2.3	0.857
12	4.0	0.966	5.6	0.959	2.2	0.849
16	4.2	0.955	5.5	0.942	2.5	0.820
22	3.1	0.975	4.1	0.962	1.8	0.850
45	2.1	0.978	4.3	0.942	1.4	0.812
80	3.2	0.955	4.4	0.943	2.2	0.801
126	3.5	0.963	4.6	0.923	2.6	0.723
220	3.4	0.954	4.3	0.945	-	-

Reverse osmosis carried out at line pressures of 4.8 $\pm$ 0.3 atms using Durham, N. C. municipal water containing a total dissolved solids level of 8.0 $\pm$ 0.5 x 10^{-5} g/cm^3 and a pH of 6.7 $\pm$ 0.7 with a temperature range of: $12 \leq t, ^\circ C \leq 26$.

A typical flux-time curve for a Polymer I membrane operating with seawater is shown in Figure 3. A steady-state decline in flux (d log J_1/d log t = -0.112) is observed for the first 35 days of operation, at which time a rapid increase in the rate of decline is observed. This abrupt rate change corresponded to the first visible signs of test unit corrosion. An acid flush near day 68 resulted in restoration of the flux level to the original flux decay line. Again, a rapid flux decline indicates membrane fouling. The suddenness, together with persistance of the fouling, may suggest biological growth and the ability of the citric acid flush only to remove, not eliminate, it.

B. Mechanical Property Data

In addition to their chemical inertness, a salient characteristic of the aromatic polyamides and polyamide-hydrazides is their mechanical properties, especially in the presence of liquid water. While it may be difficult to correlate specific physical property data to long-term membrane performance at high pressures, it is safe to assume that reasonable mechanical strength is necessary to withstand the high operating pressures of reverse osmosis and to provide for membrane handling. Comparative mechanical property data for Polymers I, II, V and cellulose acetate membranes are given in Table XIV. The asymmetric

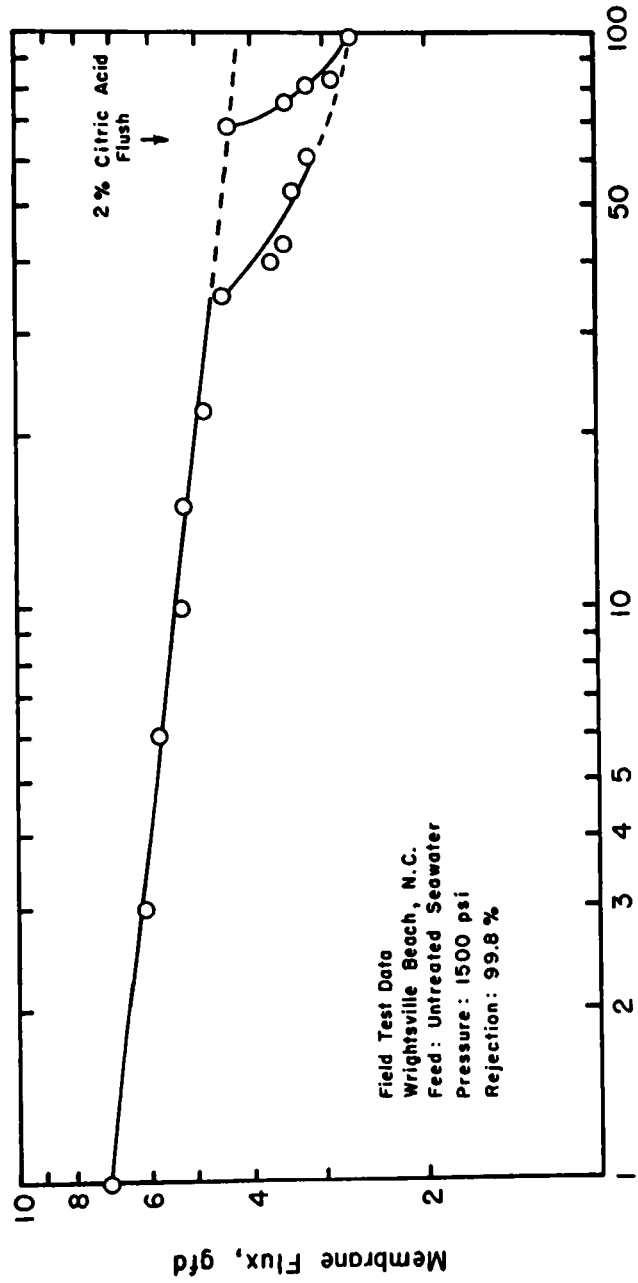

FIGURE 3
Polymer I Membrane Flux-Time Data Seawater Field Tests, Wrightsville Beach, N. C.

TABLE XIV

Comparative Mechanical Property Data for
Aromatic Polyamide Membranes

	Asymmetric Membranes			Homogeneous Membranes		
Polymer	Modulus (psi)	Yield Stress (psi)	Water Content (%)	Modulus (psi)	Yield Stress (psi)	Water Content (%)
I	82,000	2,000	54	322,000	9,100	12.3
II	-	-	-	260,000	7,700	12.6
III	82,000	2,800	52	-	-	-
V	250,000	7,100	28	348,000	9,700	10.4
Cellulose Acetate	33,000	780	-	162,000	3,700	15.6

Mechanical property measurements carried out on an Instron tester at 24 $\pm$ 1° C with the membrane positioned underwater.

film is Eastman's R097, the homogeneous film was prepared for a solution of Eastman's E398-3 polymer in acetone. The all-para structured, polyamide-hydrazide polymer (Polymer V) possesses the greatest strength in both asymmetric and homogeneous membrane form. It also has the lowest equilibrium water sorption values of the homogeneous films tested indicating a reduced level of plasticizing at test conditions.

C. Membrane Structure

A detailed study, of the structure of aromatic polyamide and polyamide-hydrazide membranes, has been carried out with the aid of the transmission electron microscope. A major obstacle encountered in membrane pore structure studies was that of sample preparation. Initial experiments indicated conventional freeze-drying techniques would not permit retention of the fine pore structure of the membranes. A chemical exchange process, ending in the membrane being filled with a methacrylate embedding material, provided the necessary pore-structure stability. These stabilized membranes were then sectioned in a Reichert © Ultramicrotome equipped with a diamond knife. Cross-sections approximately 200-400 Å thick were obtained by this method. These sections were picked up on a carbon-coated grid and examined in a Philips Model EM200 Transmission Electron Microscope at magnifications up to 71,000X.

Membrane anisotropy is indicated from the electron micrographs in Figure 4 and 5. The photomicrographs reveal the fine structure of the air dried (skin or selective side) and bottom surfaces, respectively, for a high flux Polymer I membrane. Casting streaks are evident in the otherwise smooth texture of the air dried surface. The membrane bottom (the side in contact with the glass plate) is comparatively rough indicating the highly irregular nature of the more porous membrane matrix.

An electron photomicrograph of a Polymer I membrane cross-section taken at 71,000X is shown in Figure 6. A close examination of this figure reveals a skin or dense region, about 350 Å thick, at the air dried surface and supported on a matrix containing voids. The voids appear to be of two distinct sizes. The larger ones, identified as macropores, are approximately 140 Å in diameter whereas the smaller pores (micropores) are at the limit of resolution for the electron microscope (ca. 15 Å). The 350 Å observed skin thickness is in good agreement with that predicted (300 Å) from homogeneous membrane data (see Table I) based on a water permeability (P_1) of 2.8×10^{-8} g/cm^2-sec.

A detailed representation of the entire cross-section of a high flux Polymer I membrane is given in Figure 7. The rectangles in Figure 7 represent mapped regions, from which detailed enlargements of about 71,000X, shown in Figures 7-1

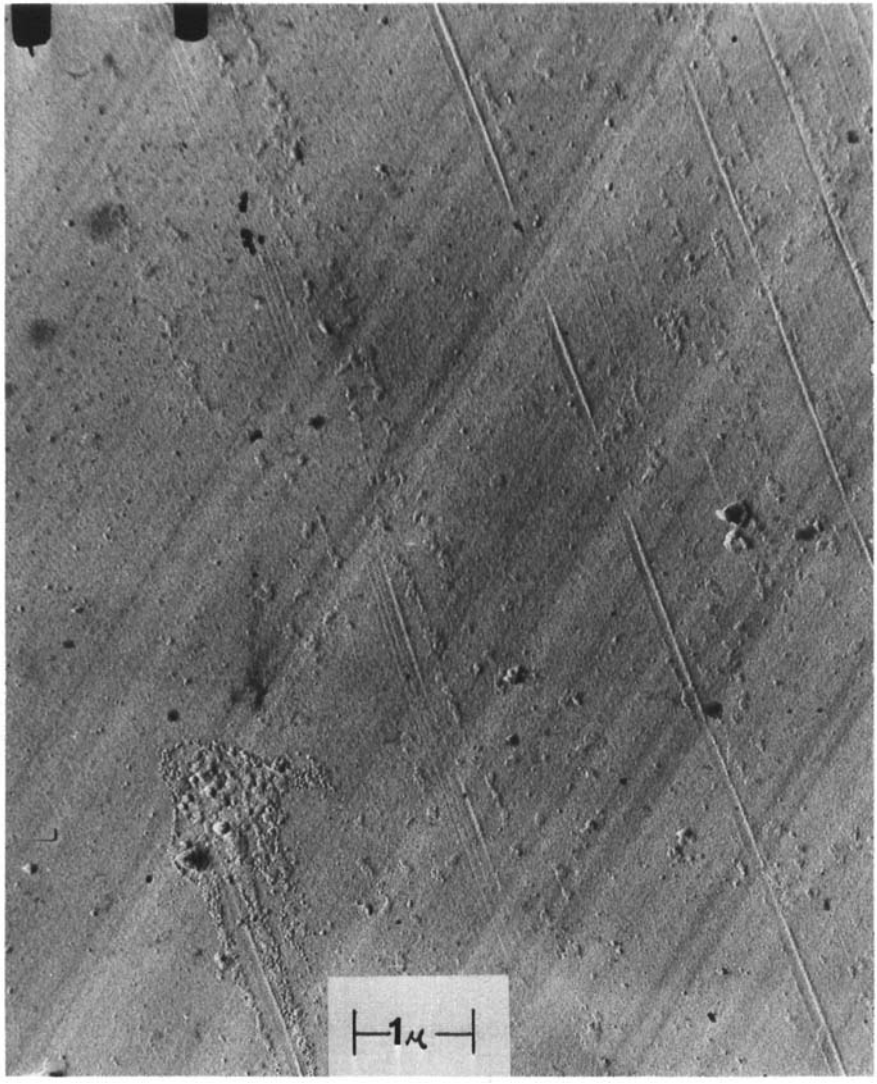

FIGURE 4
Electron photomicrograph of a preshadowed carbon-platinum replica of the air-dried surface of an asymmetric Polymer I membrane

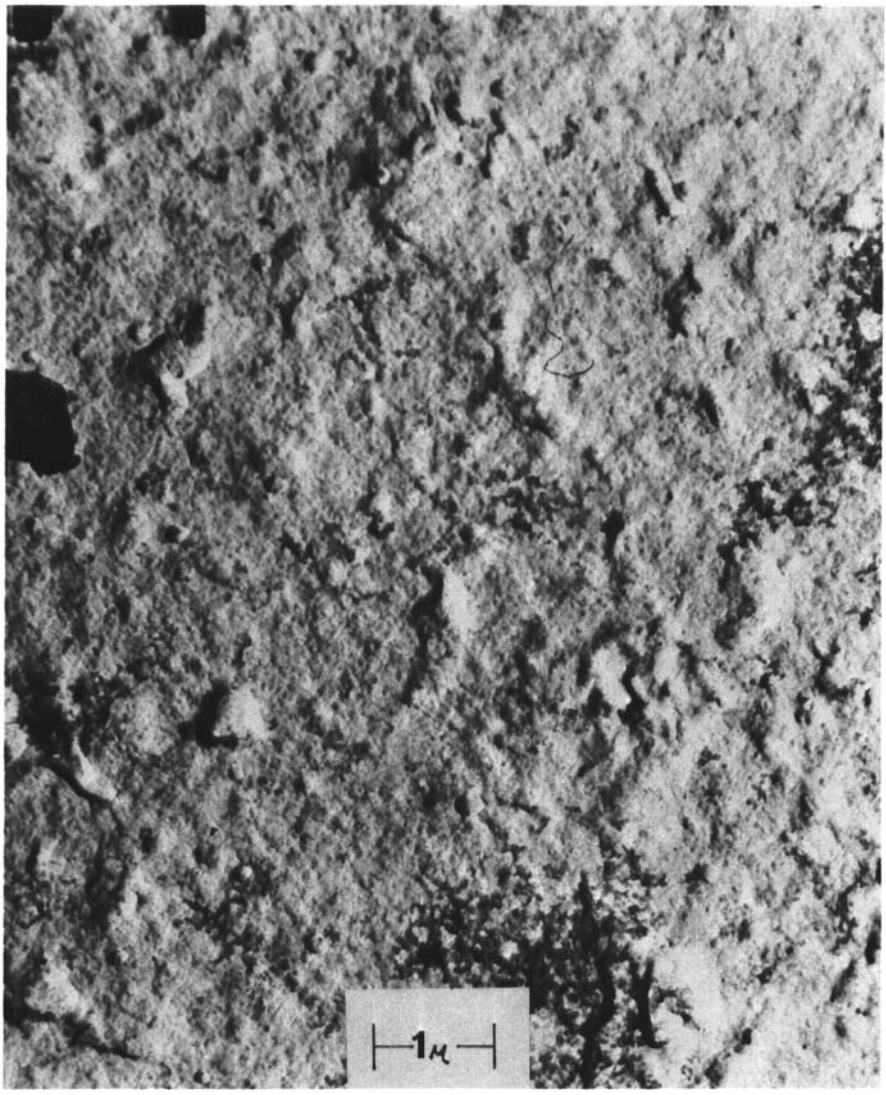

FIGURE 5
Electron photomicrograph of a preshadowed carbon-platinum replica of the bottom surface of an asymmetric Polymer I membrane

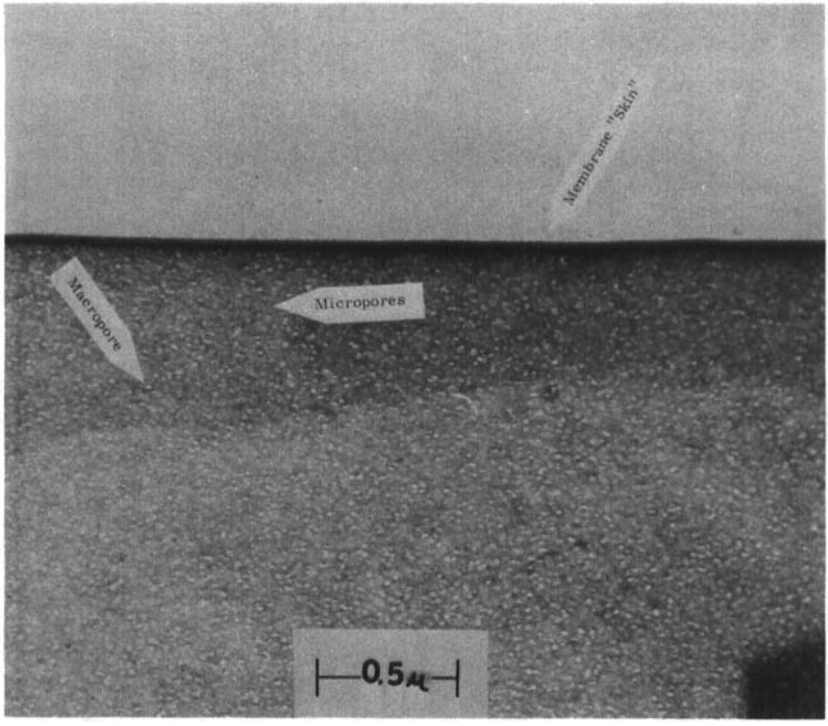

FIGURE 6
Electron photomicrograph of the skin region of an asymmetric Polymer I membrane cross-section

through 7-9, were made. Figure 7-1 is an enlargement of the membrane bottom surface, that is, the surface in contact with the glass plate during the oven drying interval. Note that this region appears completely devoid of any pore structure larger than 30 Å and, in fact, appears to show the rudiments of a skin. This complete absence of large pore structure is believed to result from extremely low coagulation rates for this portion of the membrane,

as previously discussed in this chapter. The second area (Figure 7-2, bottom portion) from the membrane bottom, shows the same high matrix density, previously observed in Figure 7-1. The uppermost portion of this region shows some indication of pore enlargement (ca. 60 Å). In Figure 7-3 the same pore-size and distribution, found in the upper portions of Figure 7-2, are seen. Figure 7-4 shows macropore dimensions near the 60 Å size, but at a much higher concentration than observed in the previous regions. An increase in pore size becomes evident in Figure 7-5. Note the position of the dense (dark) region (a fold or overlap in the cross-section) of Figure 7-5 in relation to the entire membrane cross-section shown in the mapped section (Figure 7). The size of the macropores is seen to steadily increase (Figures 7-6 and 7-7) as the enlarged areas approach the air dried surface, reaching a maximum of 300 Å in the region corresponding to Figure 7-8. Also in this region, a few very large (ca. 0.3 micron) voids are seen. As the air dried surface is reached (Figure 7-9) the number and size of the macropores are reduced. Again, we see a skin approximately 300 Å in thickness. The lack of appreciable large pore structure in the region or band below the skin is not too dissimilar from that observed by Gittens et al.[15], for cellulose acetate. The dense bottom region, while unusual for cellulose acetate, has been observed[16] in mem-

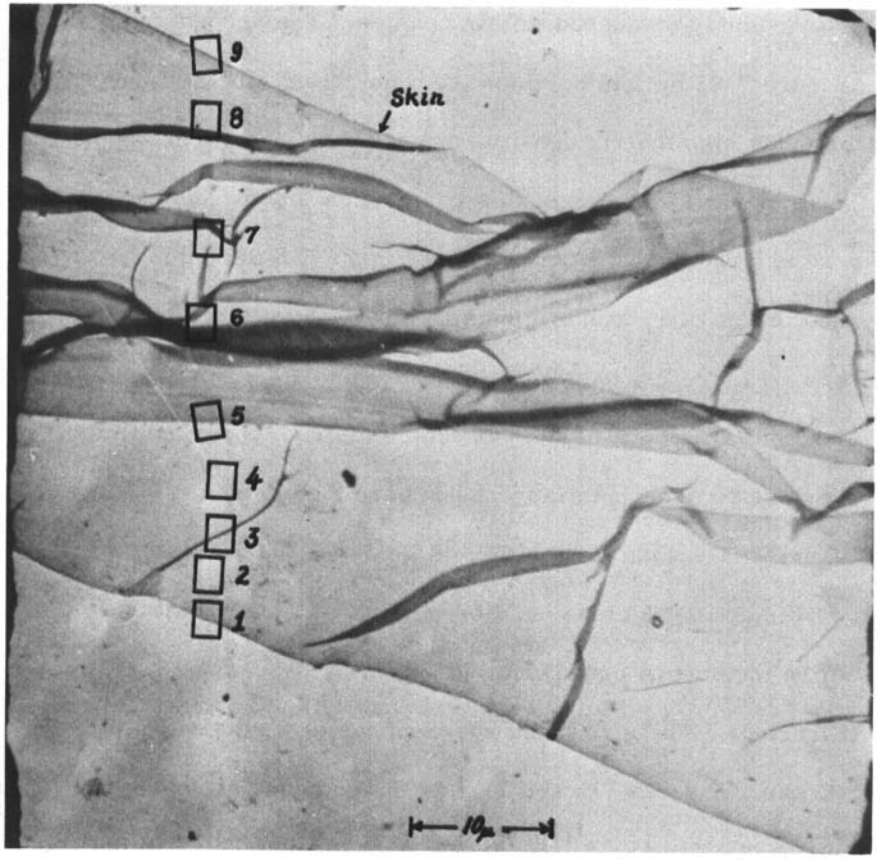

FIGURE 7
Electron photomicrograph indicated mapped regions of enlargement for an asymmetric Polymer I membrane cross-section

branes prepared from solutions of that polymer in dimethyl-formamide. Similar to cellulose acetate is the structure observed for the coagulated (25° C) Polymer V (polyamide-hydrazide) membrane illustrated in Figure 8. A gradual increase in pore size is observed beginning at the top and continuing to the

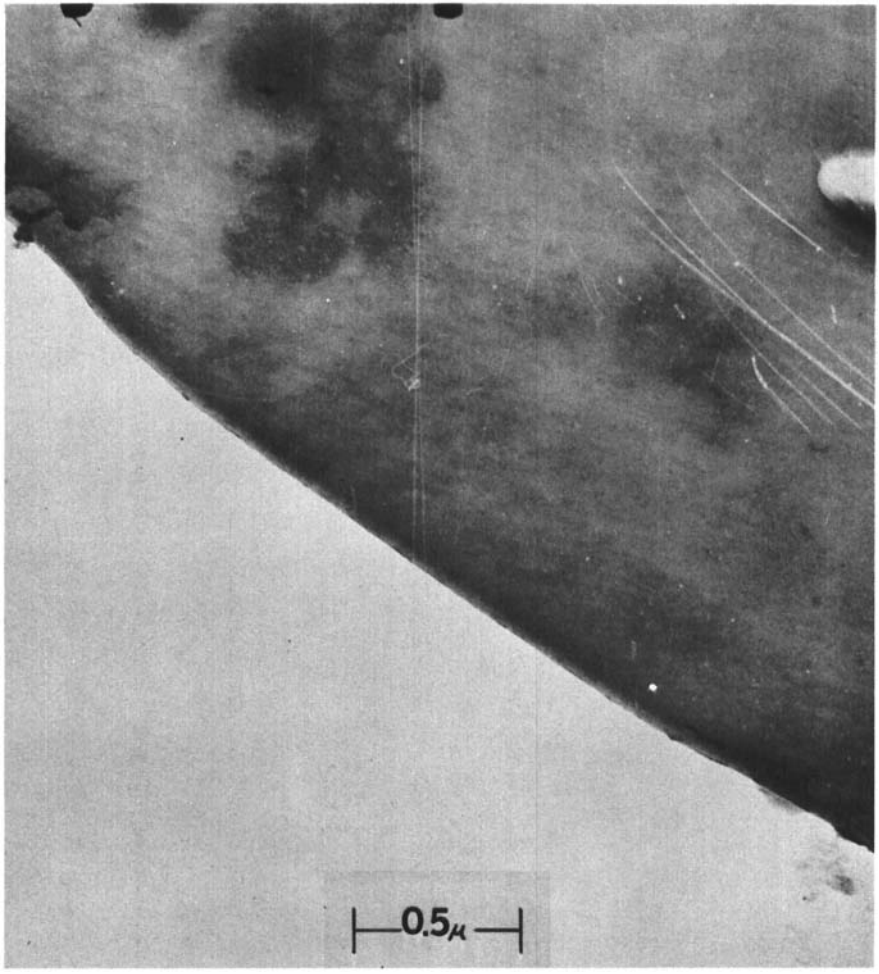

FIGURE 7-1
Mapped area-bottom surface region of the membrane cross-section

bottom surface of the membrane section. At the top surface there exists a rudimentary skin, formed during the oven drying step. Such a membrane would have a sodium chloride rejection

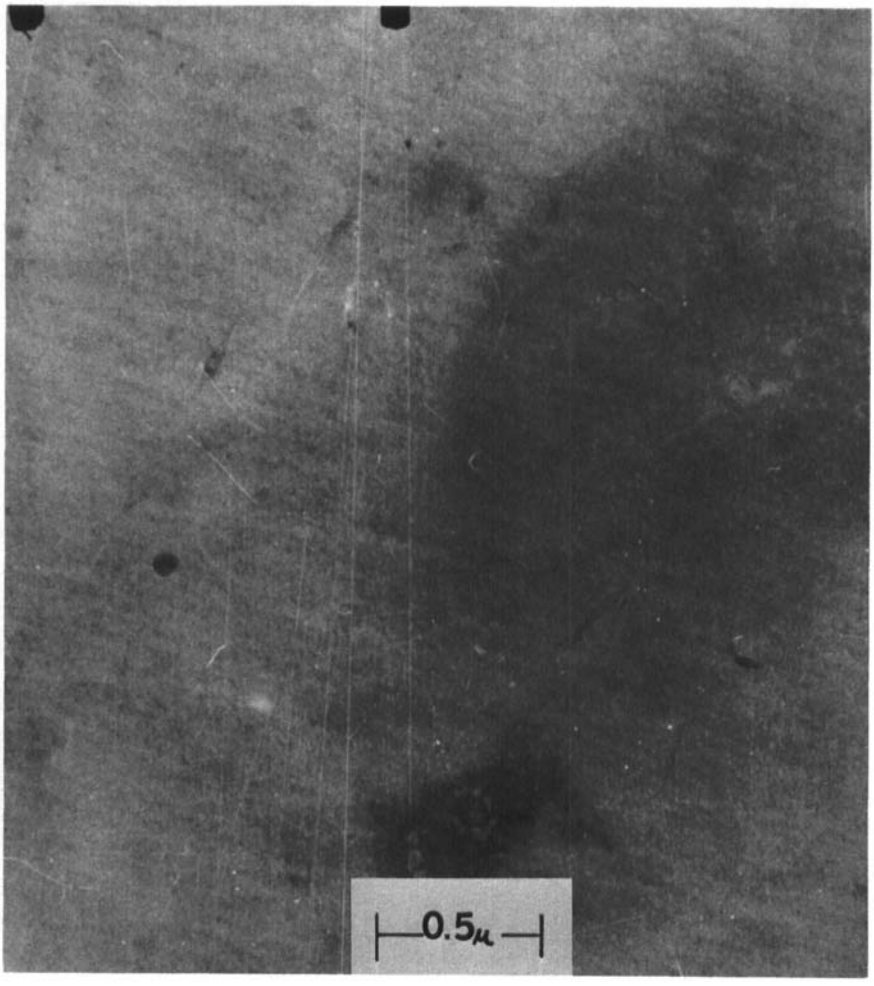

FIGURE 7-2
Mapped area-membrane interior cross-section

of only 0. 6 and a flux of 14 x 10^{-4} g/cm^2-sec at an operating pressure of 41 atms.

Annealing this membrane (Polymer V) for 15 minutes in boiling water results in a significant densification in the mem-

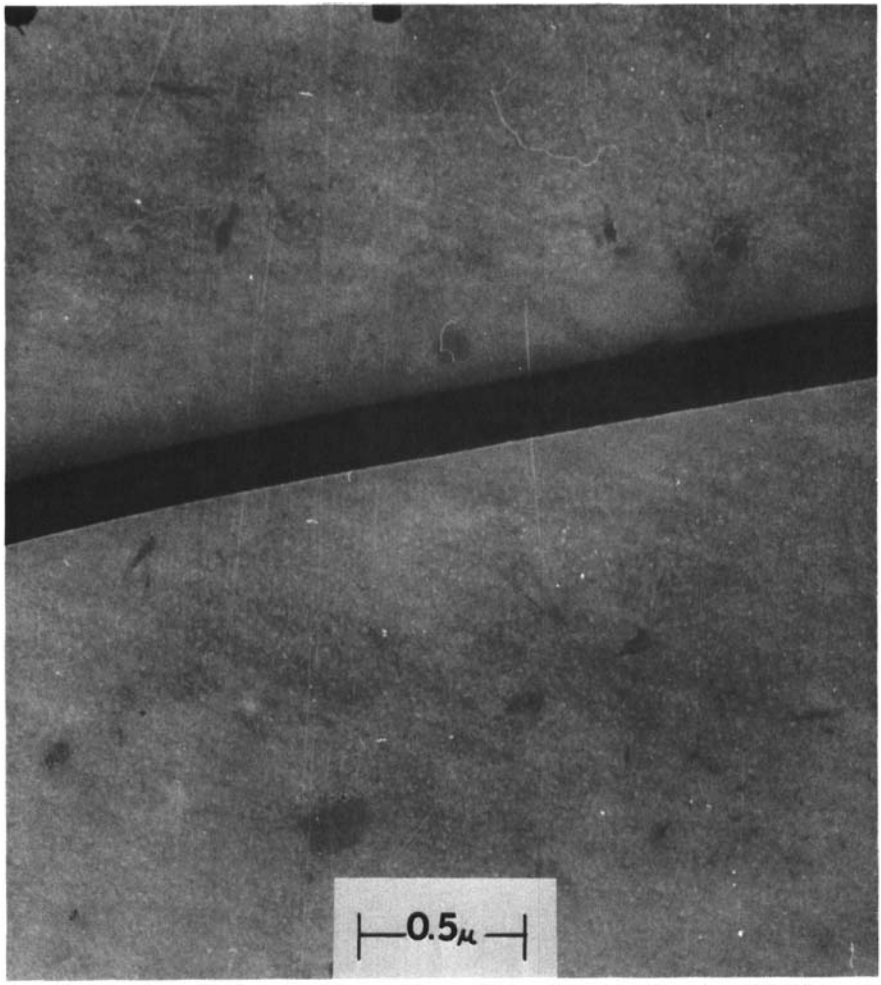

FIGURE 7-3
Mapped area-membrane interior cross-section

brane skin region shown in Figure 9 and a subsequent improvement in selectivity to sodium chloride and a reduction in flux. This membrane provided a flux of 9.4×10^{-5} g/cm^2-sec and a rejection of 0.98.

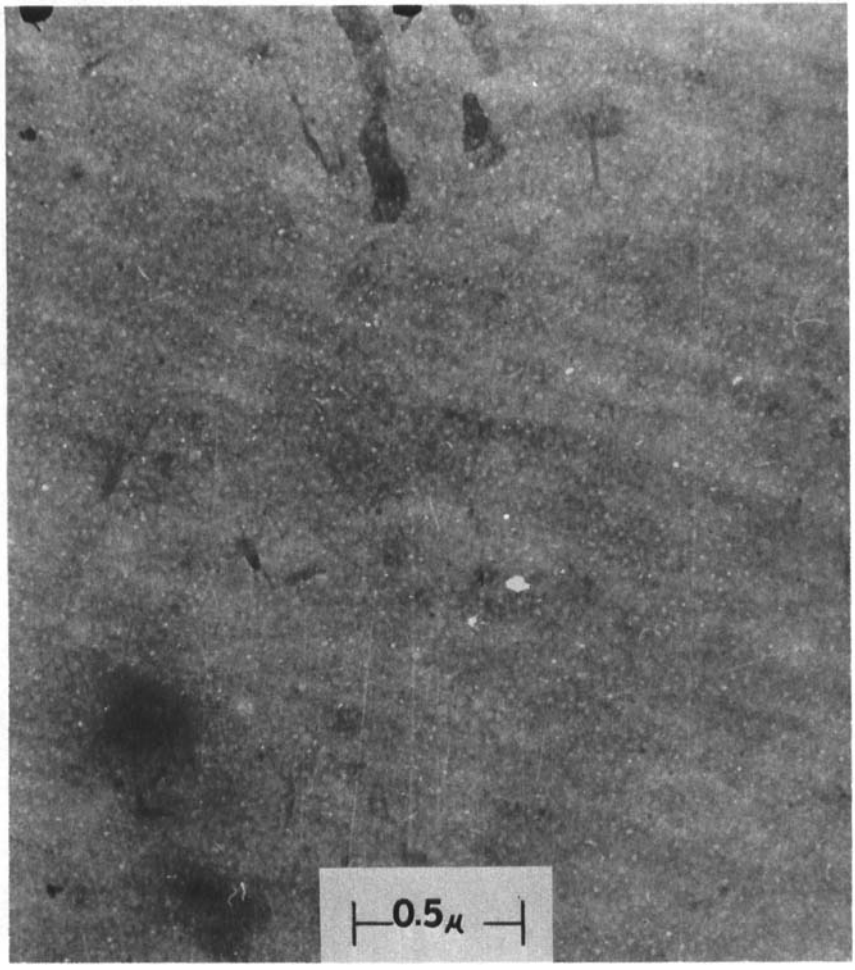

FIGURE 7-4
Mapped area-membrane interior cross-section

Coagulation temperature is an important variable in controlling membrane porosity. Polymer V membranes coagulated in ice water mixtures have large open pore structures as illustrated by Figure 10. The existence of a pore-size gradient is

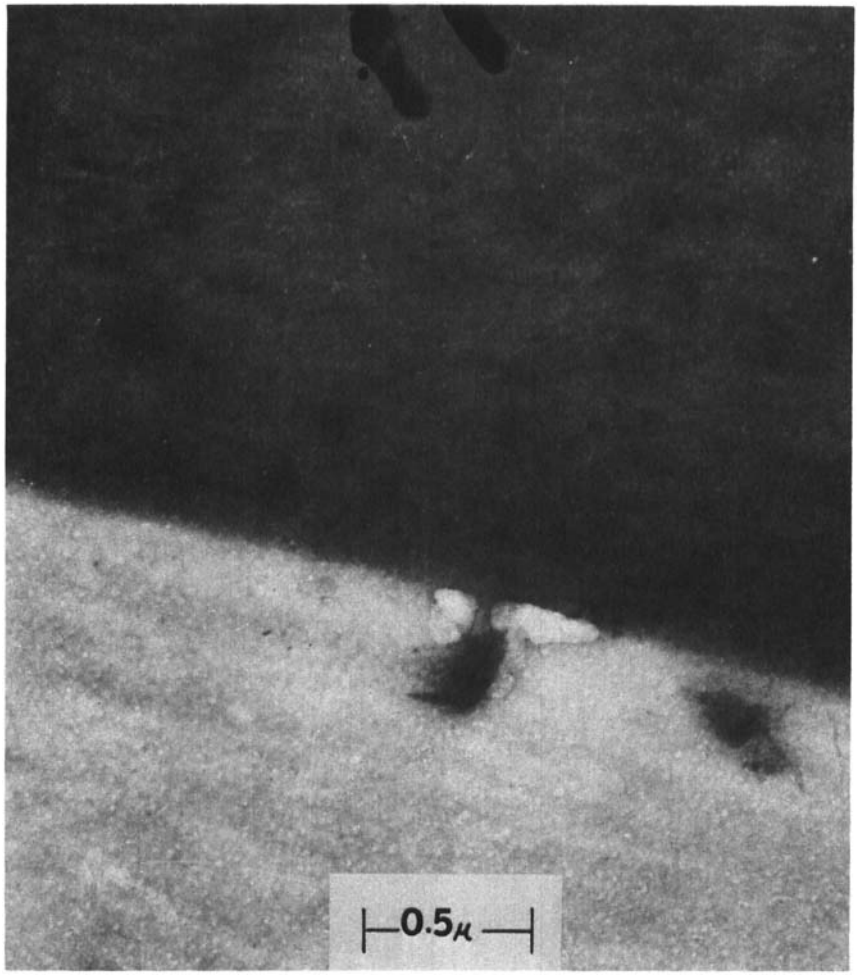

FIGURE 7-5
Mapped area-membrane interior cross-section

evident,with the larger pores (ca. 0.25 micron) prevalent in the interior portion of the matrix. Ambient temperature coagulation (Figure 8) results in an equally porous matrix but generally smaller pores. High temperature coagulation (ca. 50° C) results

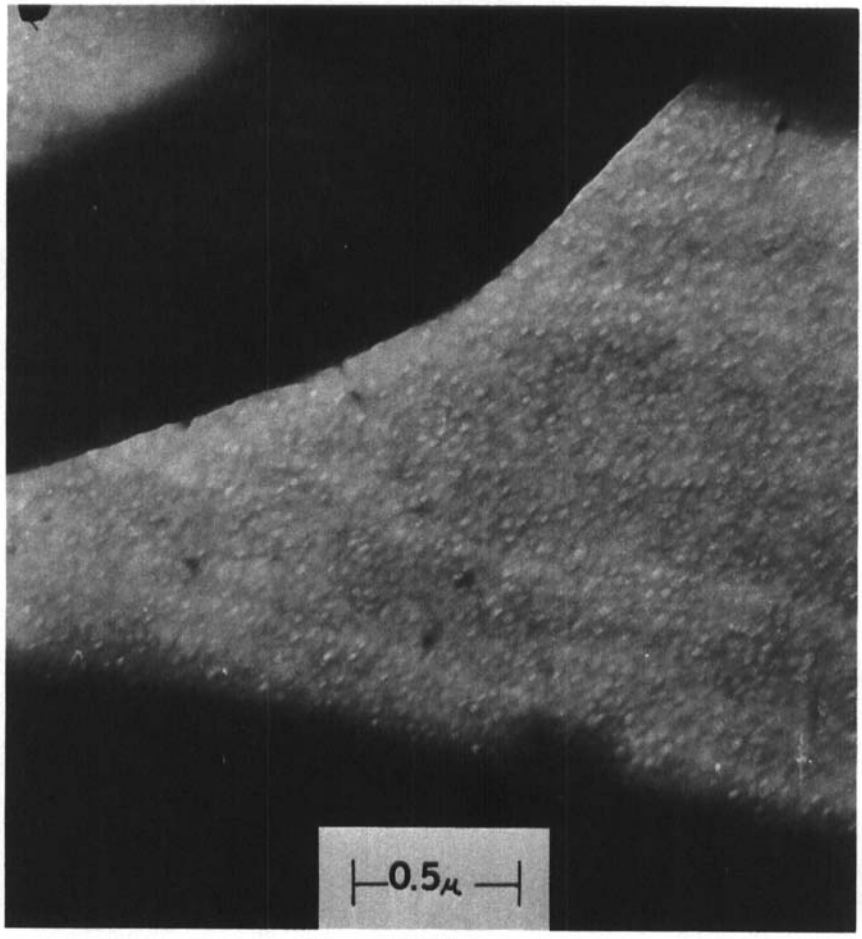

FIGURE 7-6
Mapped area-membrane interior cross-section

in the collapsed, dense structure shown in Figure 11. Pore diameters for this membrane are approximately 0.05 micron.

The polyamide membrane from Polymer I shows an extremely even distribution of pores, approximately 200 Å in

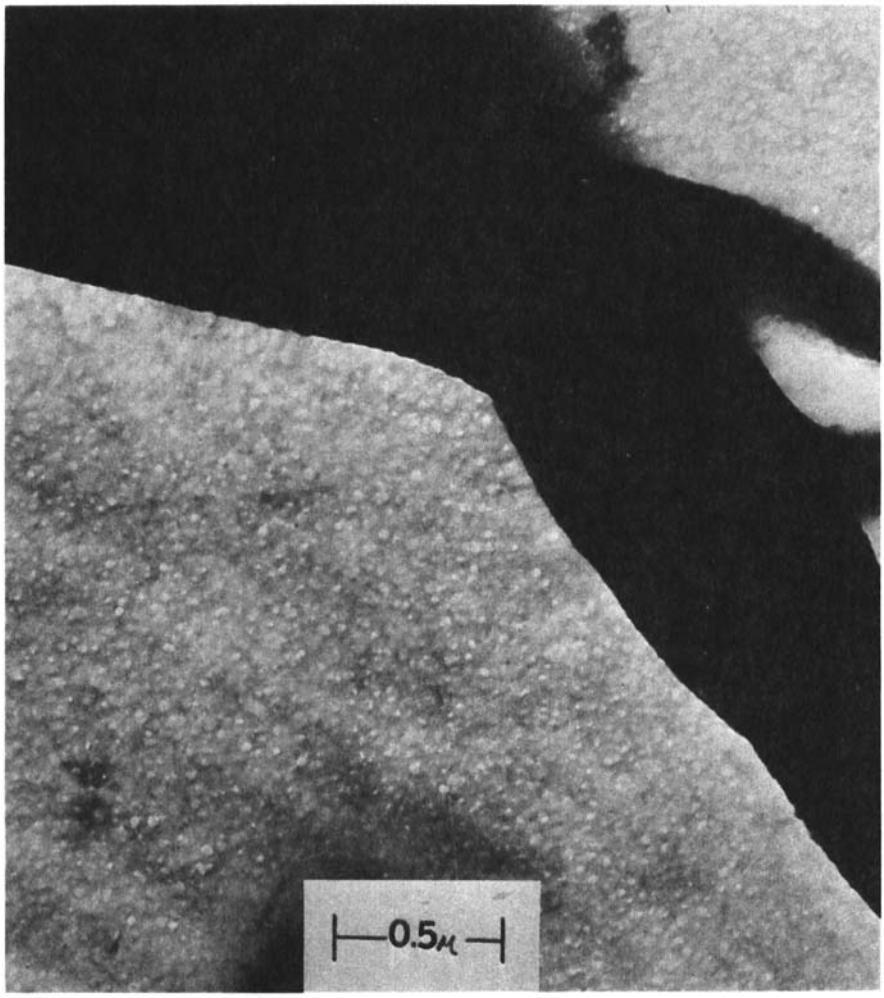

FIGURE 7-7
Mapped area-membrane interior cross-section

diameter, when coagulated in ice water as shown in Figure 12. Coagulation of this polymer in 45° C water results in pores close to 500 Å in diameter as illustrated by Figure 13. The increase

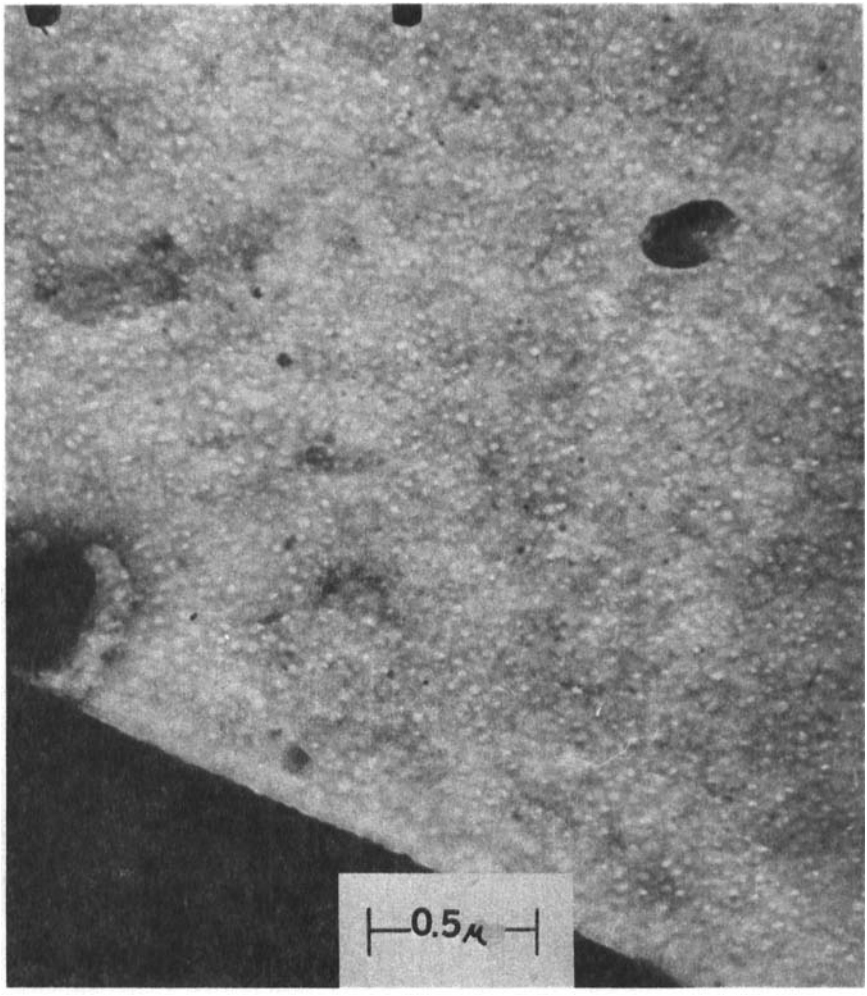

FIGURE 7-8
Mapped area-membrane interior cross-section

in pore size is believed to occur, in part, as the result of membrane crystallization. Such explanation is consistent with observed reverse osmosis performance. Polymer I membranes

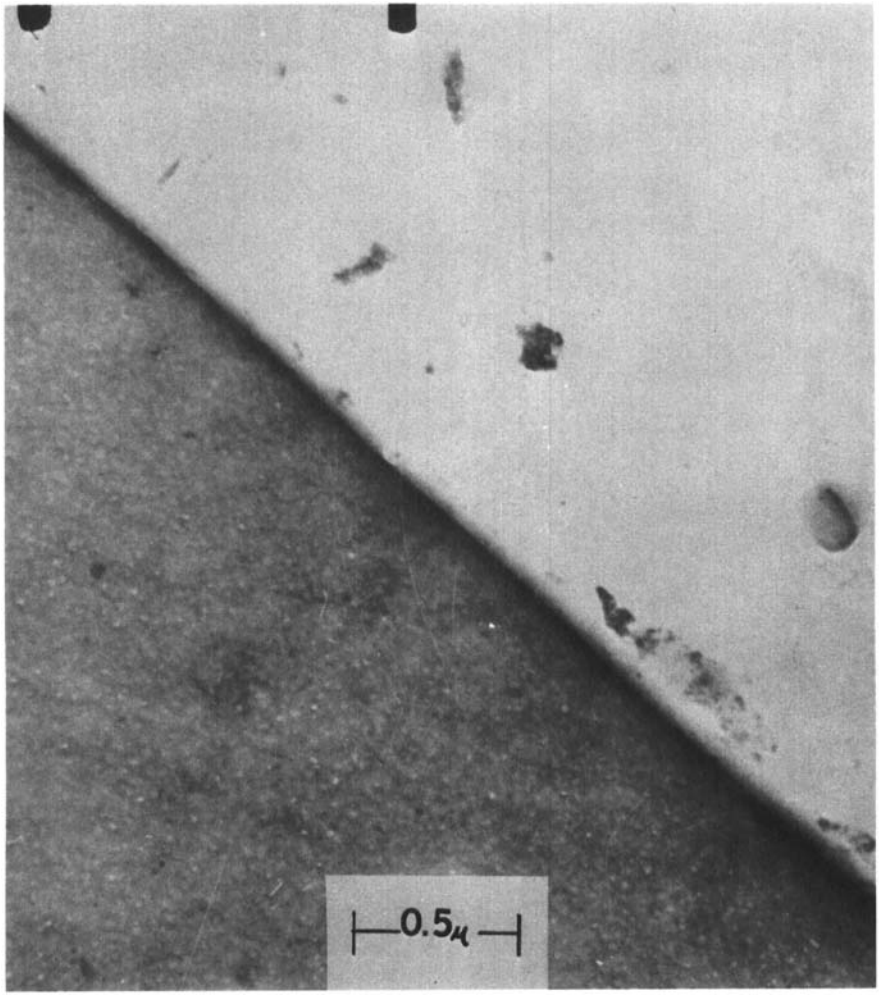

FIGURE 7-9
Mapped area-membrane air-dried surface region

coagulated at this temperature generally show poorer selectivity. For example, heating Polymer I membranes in water results in an increase in flux with a decrease in selectivity.

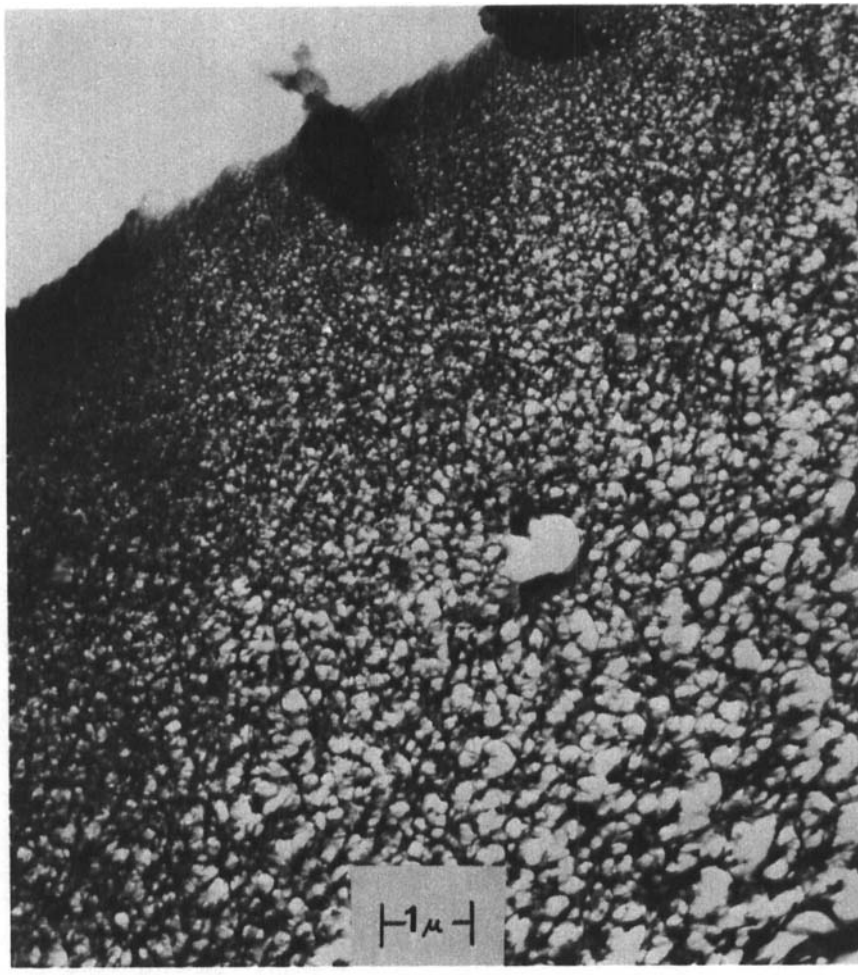

FIGURE 8
Electron photomicrograph cross-section of the air-dried surface region of an unannealed Polymer V membrane coagulated at 25° C

Electron micrographs of Polymer II membranes indicate the existence of a density gradient within the membrane skin (Figure 14). There exists a region of low density at the outer-

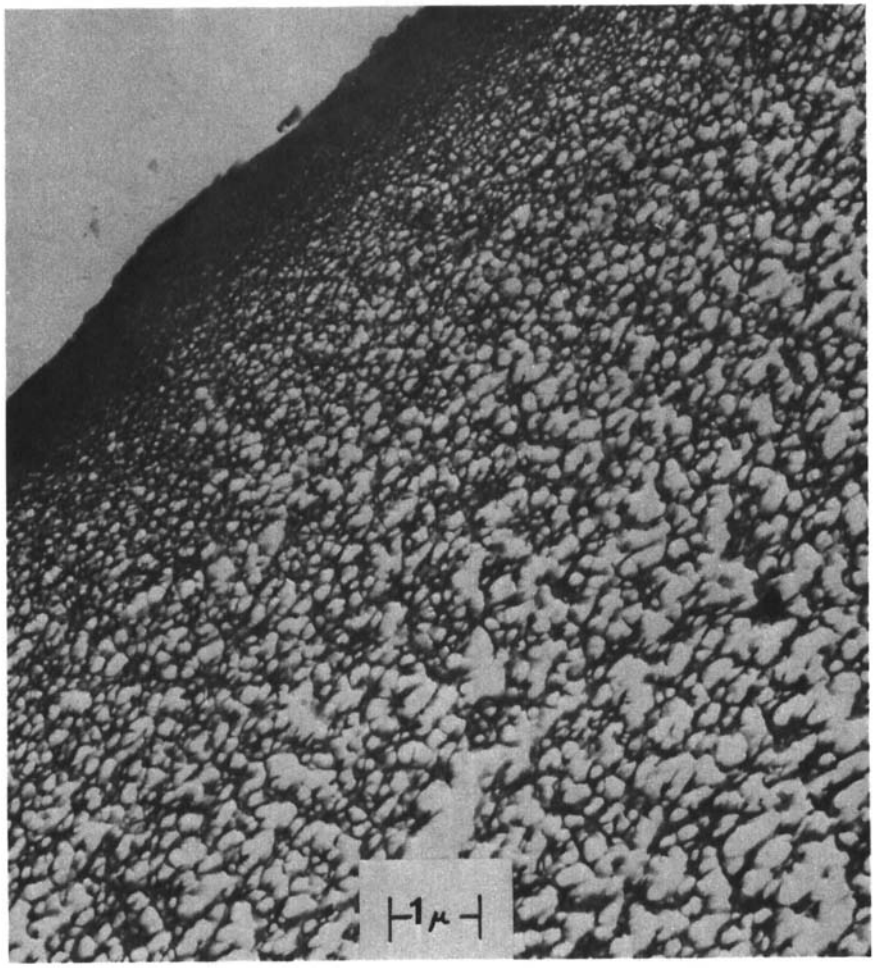

FIGURE 9
Electron photomicrograph cross-section of the air-dried surface region of an annealed Polymer V membrane coagulated at 25° C

most surface (air-dried side) supported on a very dense layer approximately 280 Å thick. The entire band is nearly 1000 Å thick. Transport data indicate the effective thickness (for water transport) to be an intermediate value.

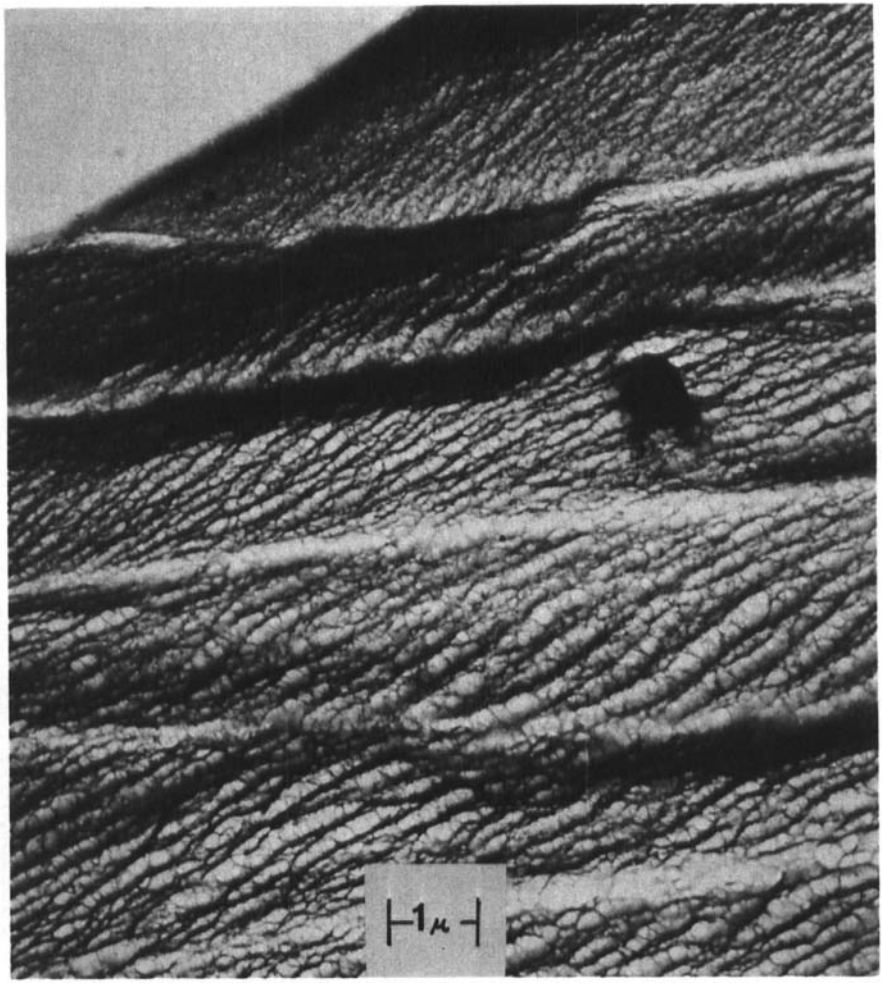

FIGURE 10
Electron photomicrograph cross-sections of the air-dried surface region of an unannealed Polymer V membrane coagulated at 0° C

In addition to cause and effect observations for preparative variants and membrane structure studies, electron microscopy has proven to be a valuable tool in interpreting membrane reverse

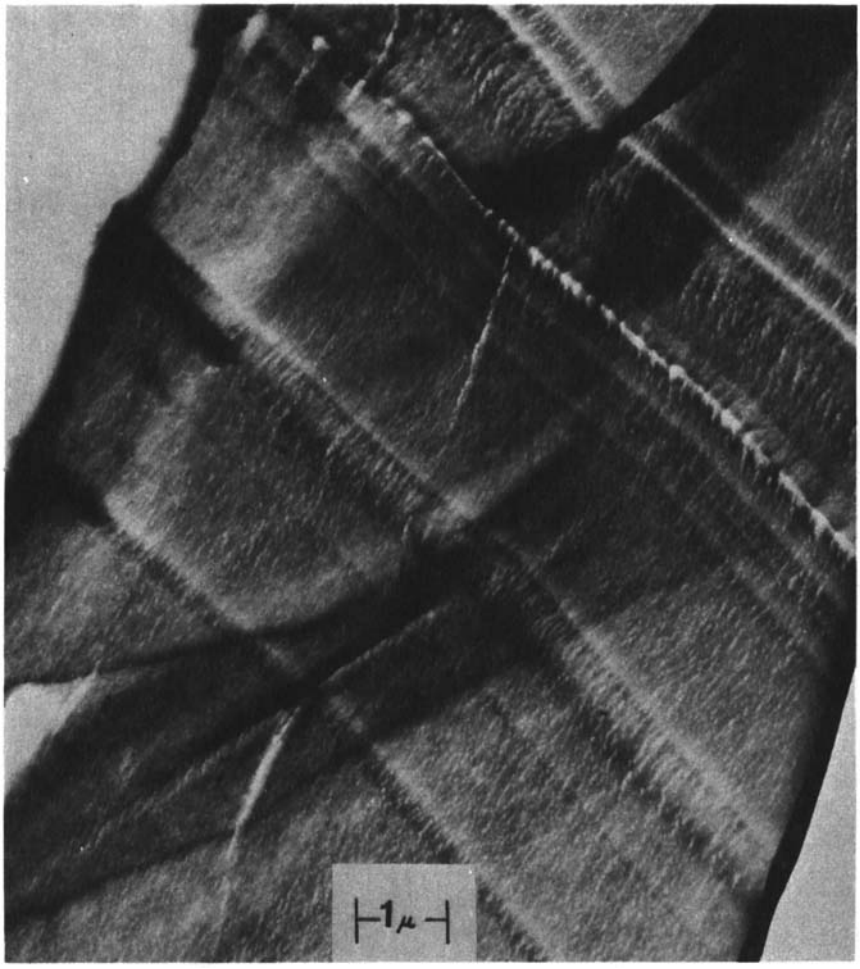

FIGURE 11
Electron photomicrograph cross-sections of the air-dried surface region of an unannealed Polymer V membrane coagulated at 50° C

osmosis behavior. For example, equilibration of an aromatic polyamide such as Polymer II in a 1M sodium chloride solution would result in approximately a 50% reduction in flux which is

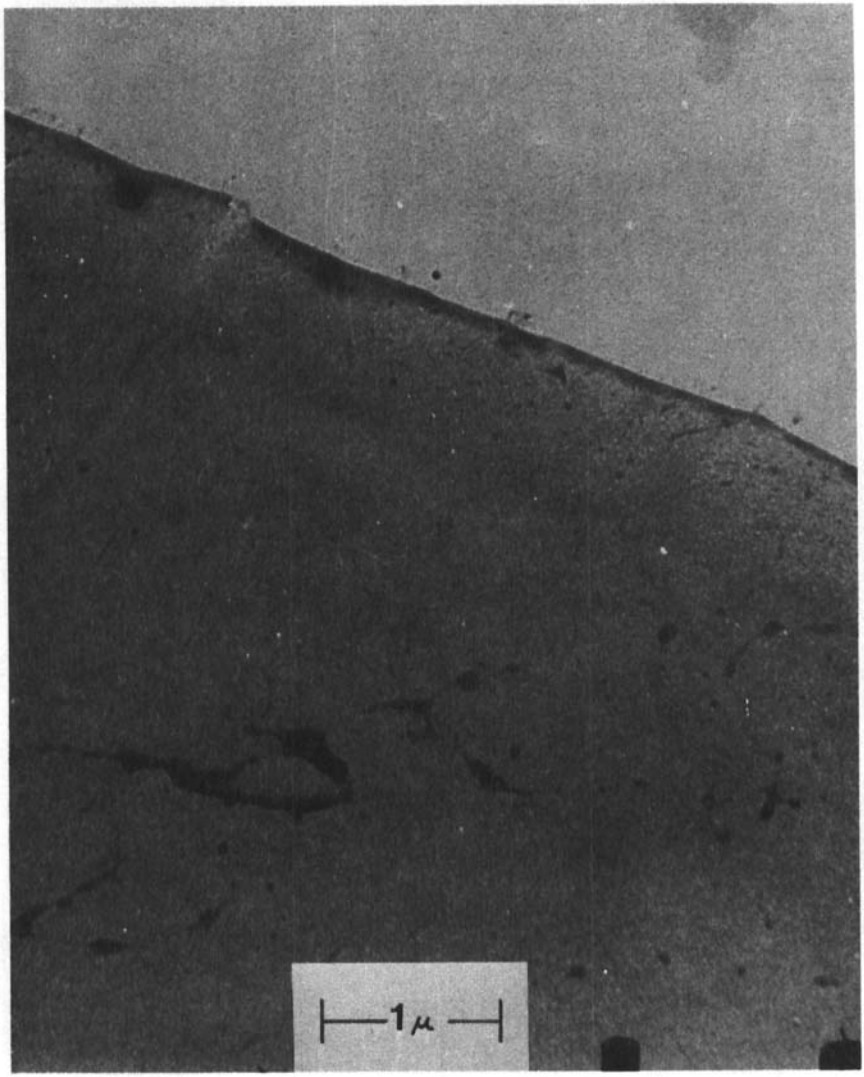

FIGURE 12
Electron photomicrograph cross-sections of the air-dried surface region of a Polymer I membrane coagulated at 0° C

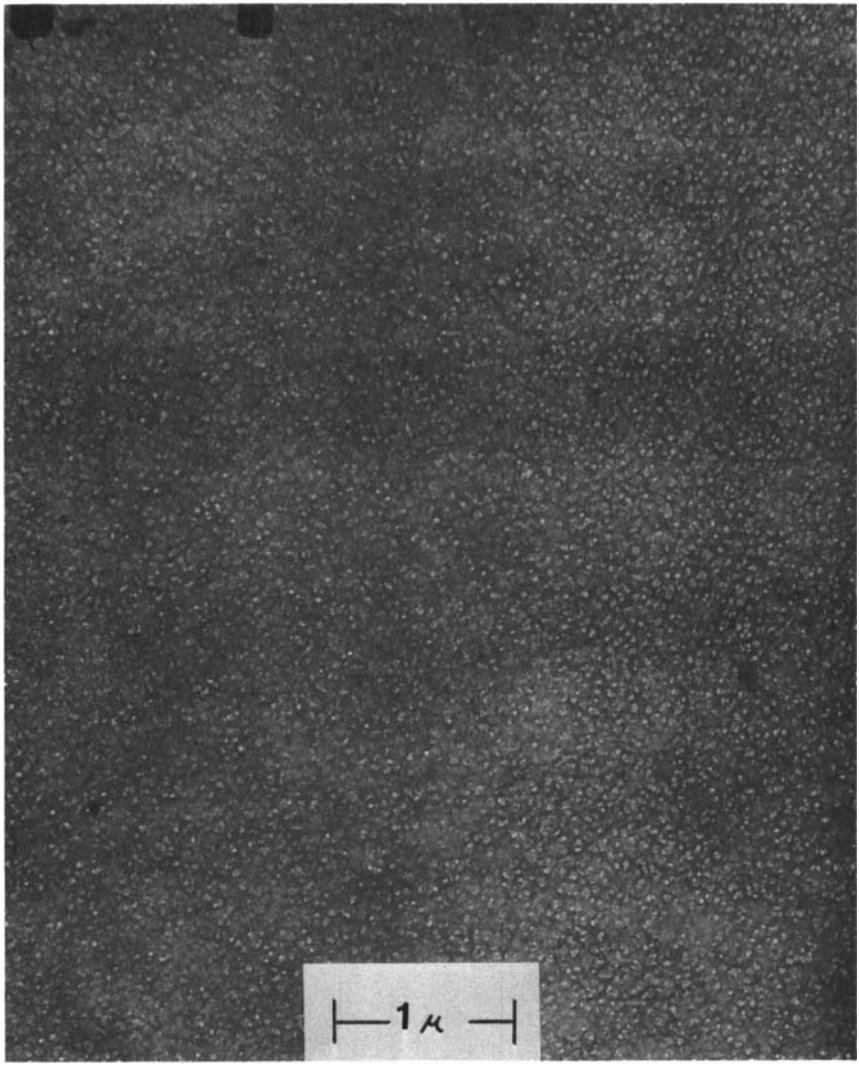

FIGURE 13
Electron photomicrograph cross-sections of the air-dried surface region of a Polymer I membrane coagulated at 45° C

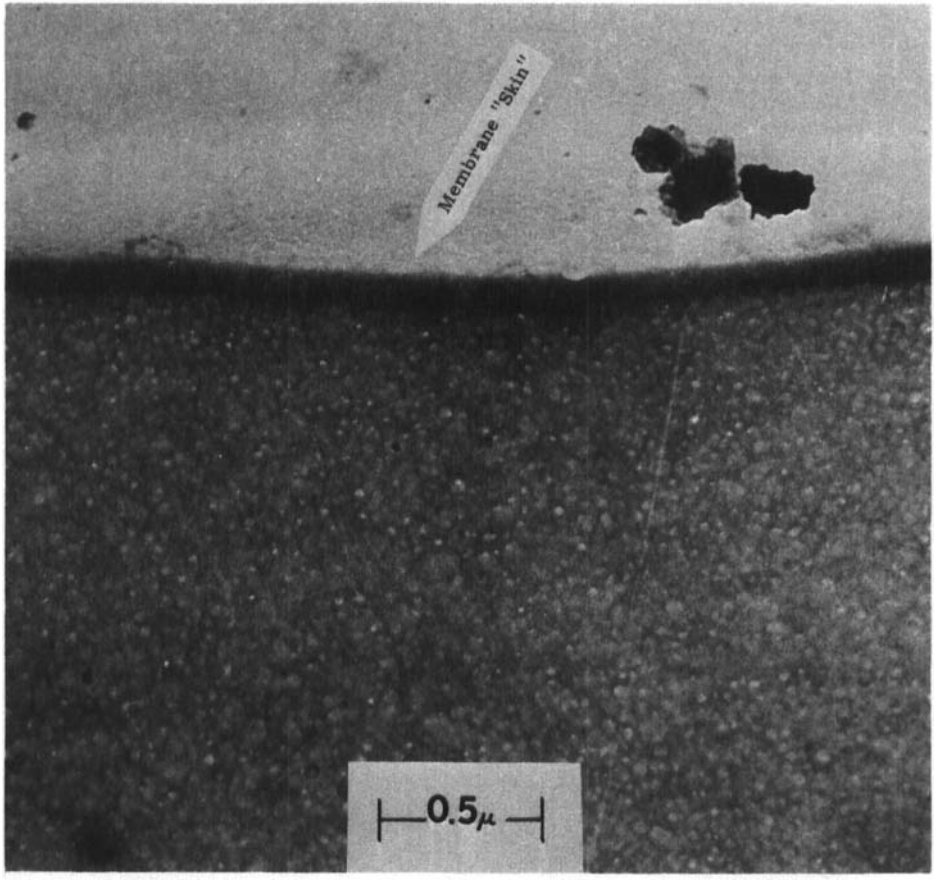

FIGURE 14
Electron photomicrograph cross-sections of the air-dried surface region of a Polymer II membrane coagulated at 25° C

non-recoverable. An examination of the cross-section of the salt equilibrated membrane in Figure 15 reveals an increase in density of the skin and matrix over the control (Figure 14), as evidenced by the loss in contrast between the skin and matrix area. Such skin densification can more than account for the observed flux decline.

A similar analysis can be applied to the understanding of membrane flux decline evident for a Polymer I membrane after 16 days operation at 102 atms with a 1.03M NaCl solution. The flux of this membrane was reduced from 4.1×10^{-4} g/cm^2-sec to 1.4×10^{-4} g/cm^2-sec over the indicated interval. An examination of the surface region (next to the salt solution) of this membrane, in Figure 16, indicates the reason for the decline. An almost complete densification of the area adjacent to the skin, and extending approximately 0.4 micron into the membrane interior, has occurred. It is obvious from thickness-normalized flux data that the effective skin thickness does not encompass the entire 0.4 micron band; nevertheless it has been substantially increased. A comparison of this dense band with the structure of an air-dried (collapsed) membrane (Figure 17) seems appropriate. Both electron micrographs reveal the equal absence of fine structure.

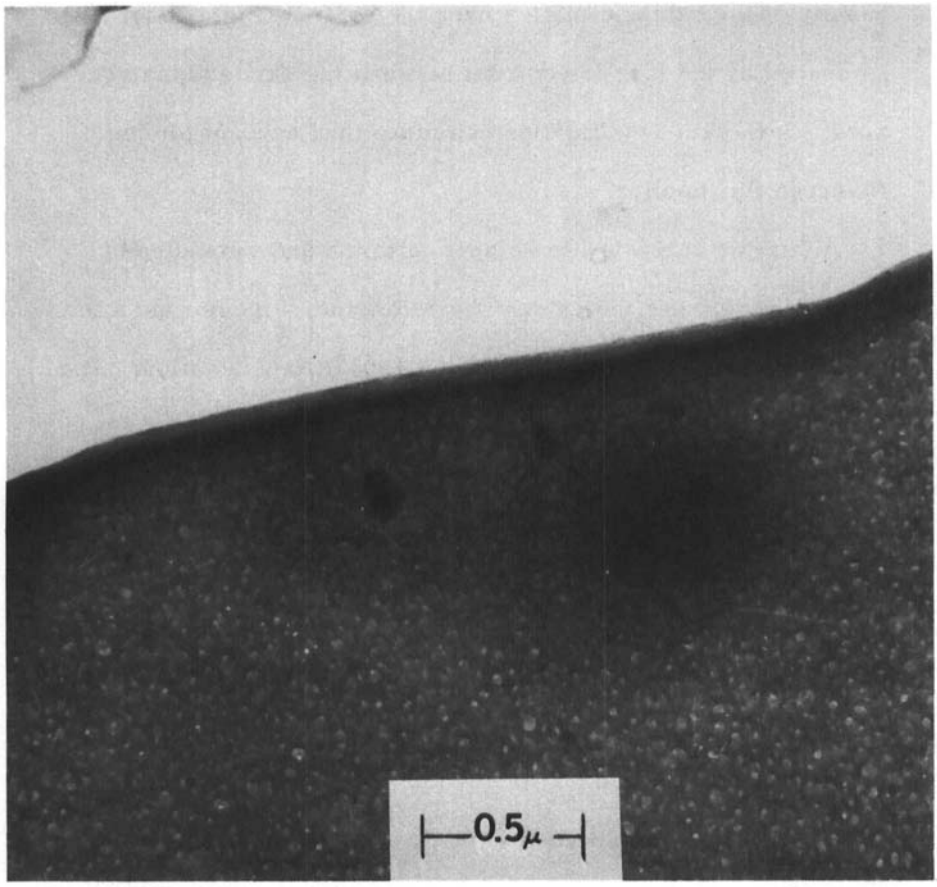

FIGURE 15
Electron photomicrograph cross-sections of the air-dried surface region of a Polymer II membrane coagulated at 25° C followed by equilibration in a 1M NaCl solution

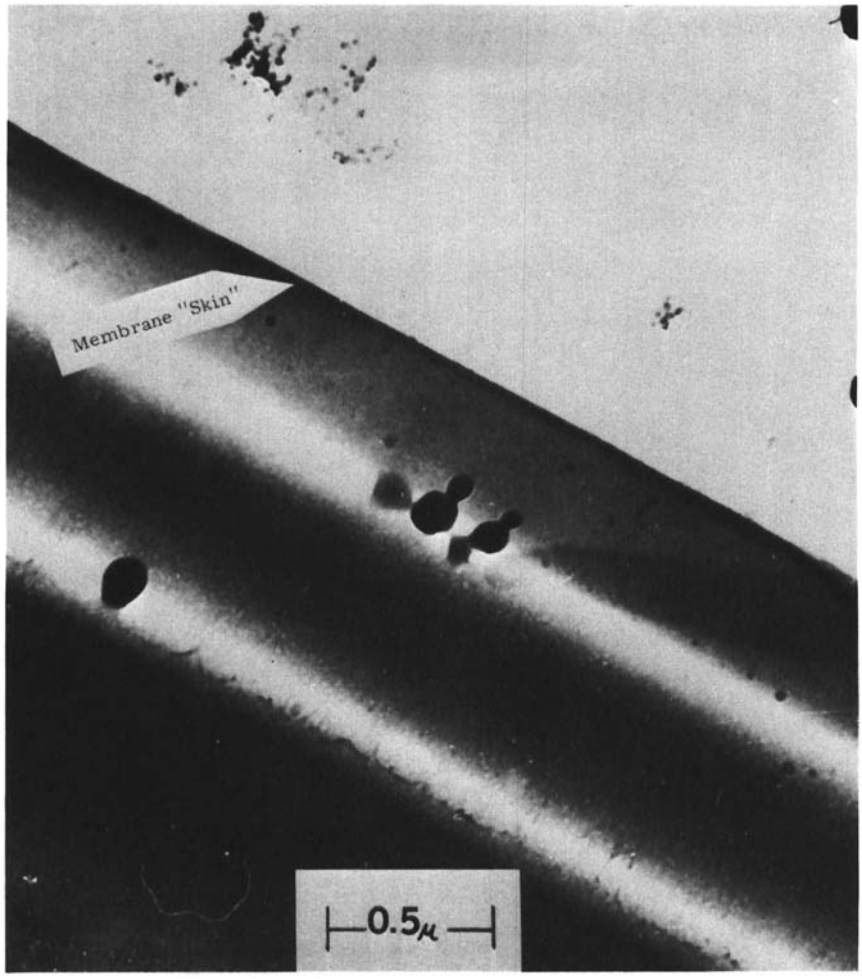

FIGURE 16
Electron photomicrograph cross-sections of the air-dried surface region of a Polymer I membrane after 16 days of reverse osmosis operation at 102 atms and a 1.03 molar NaCl solution

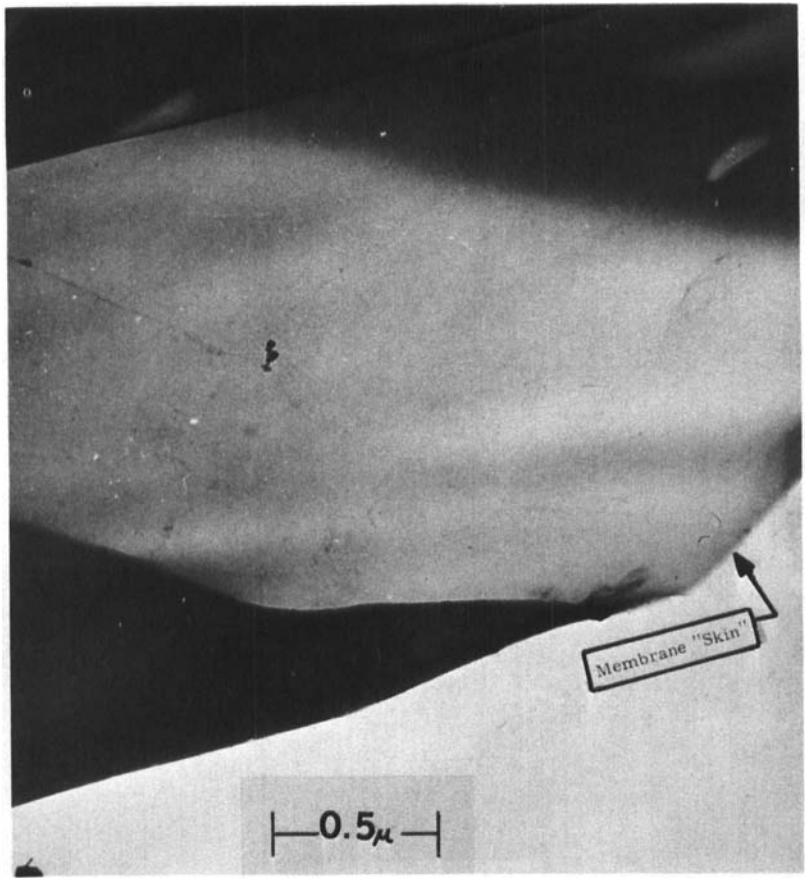

FIGURE 17
Electron photomicrograph cross-sections of the air-dried surface region of consolidated (completely dehydrated) Polymer I membrane

IV. AROMATIC POLYAMIDE TUBES AND HOLLOW FIBERS

A. Tubular Membranes

The duplication of aromatic polyamide flat film performance in seamless tubes 1.27 cm in diameter (OD) and 61 cm in length has been demonstrated.[17]

The casting procedure was a modification of the basic technique described by Loeb[18]. Polymer solution containing 0.05 to 0.20 g/cm^3 were cast to a thickness of 0.051 cm, in precision bore glass tubes with inside diameters in the range: $0.610 \leq ID, cm \pm 0.001 \leq 1.486$, with a casting bob. This casting device is illustrated at the bottom of Figure 18. The cast membrane was then placed in the specially designed oven (Figure 18) and rotated while a thermostated (105° C) nitrogen gas flow was maintained through the tube. The partially dried tube was then placed in the membrane coagulation apparatus shown in Figure 19, and washed free of solvent.

The seamless tubular membranes were then loaded into a pressure vessel, the inside of the tube filled with 1.11 cm diameter polypropylene spheres (turbulence promoters) and the membranes tested under reverse osmosis conditions.

The tubular membrane pressure vessels were one of two types. The first was constructed from type 316 stainless steel containing 4-0.05 cm holes drilled at 2.5 cm intervals, for a total of 48 holes for the 30 cm length and 72 for the 50 cm length tubes. A schematic of this type of tubular element is shown in Figure 20.

The second type of tubular pressure vessel (Figure 21) was based on a fiber glass (E glass) reinforced porous epoxy

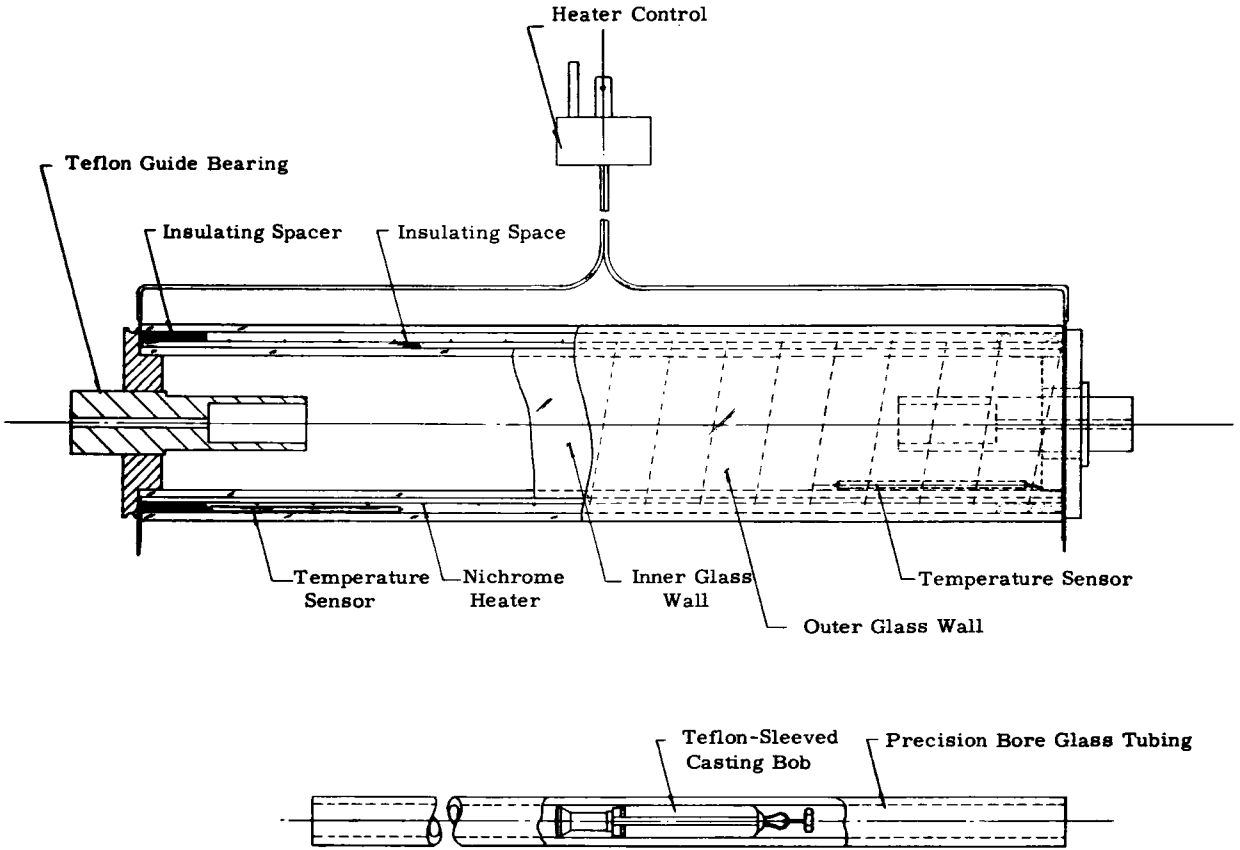

FIGURE 18
Schematic of the tubular membrane oven, precision bore glass casting tube and casting bob

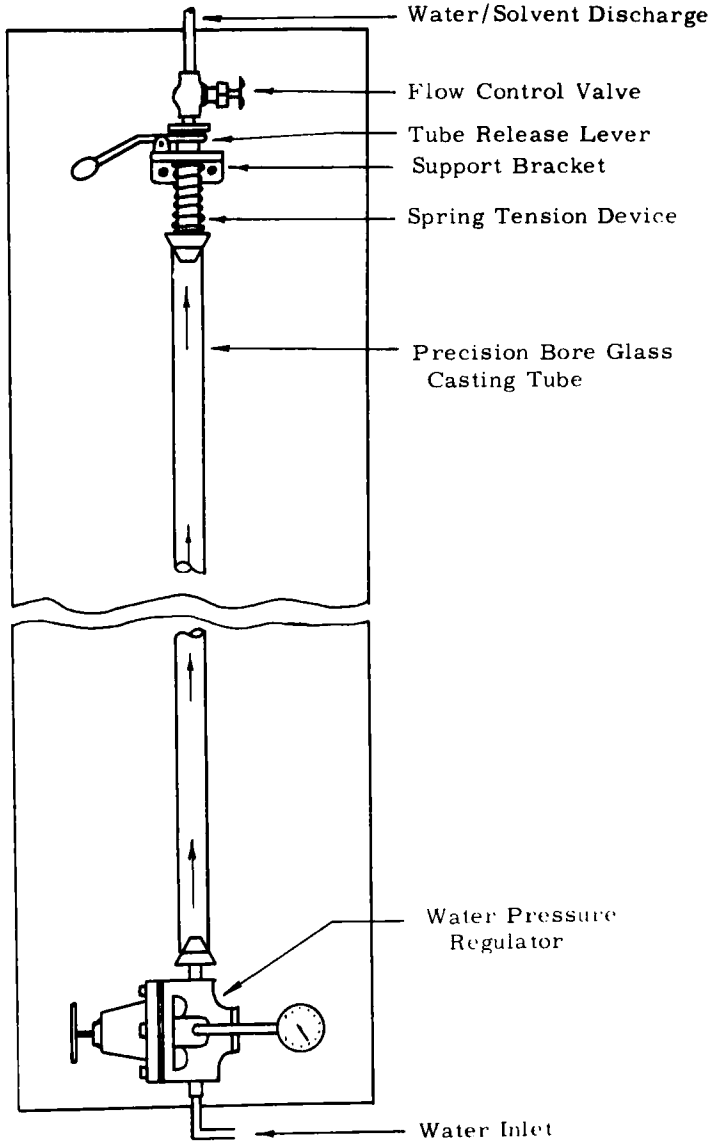

FIGURE 19
Schematic of the tubular membrane coagulation apparatus

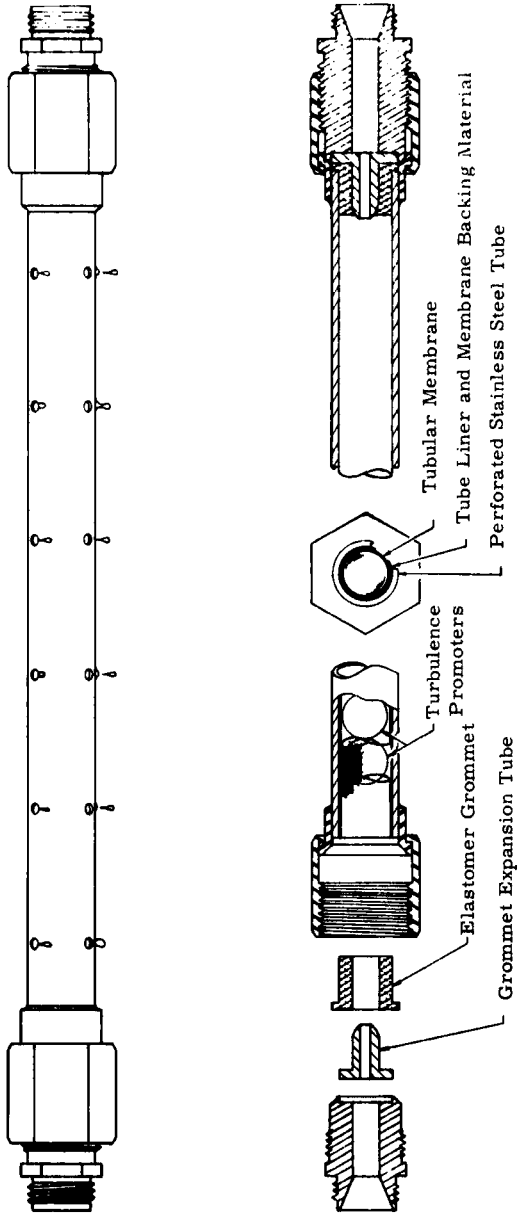

FIGURE 20
Schematic of a tubular membrane element: stainless steel type 316

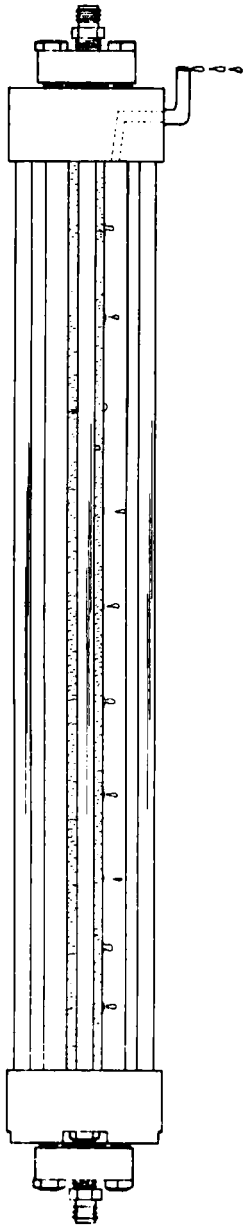

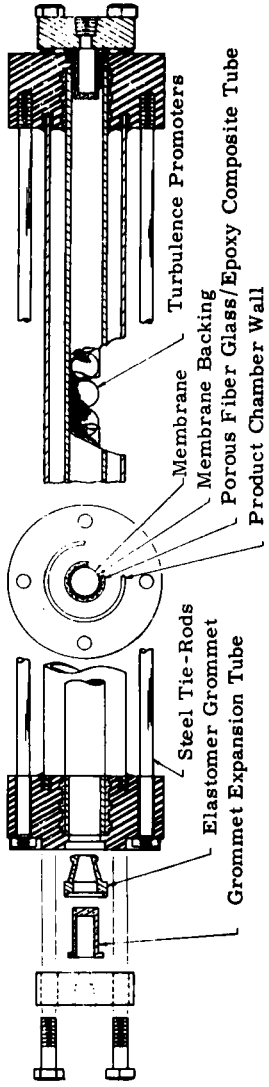

FIGURE 21
Schematic of a tubular membrane element: Fiber glass/epoxy composite type

composite tube manufactured by Hercules Corporation (ABL, Cumberland, Maryland). Both units utilized an expandable rubber grommet end seal which had been demonstrated leak-proof up to 140 atms.

The greatest difficulty encountered in the development of the tubular membrane systems has been that of tubular membrane/pressure vessel sizing and the selection of suitable membrane support or backing material.

The effects of support materials on membrane distortion under 102 atms of applied hydraulic load can best be appreciated visually. Scanning electron photomicrographs (SEM) of two identical tubular membrane surfaces together with their supports, after 48 hours of reverse osmosis operation at 102 atms are shown in Figures 22 through 25.

Figure 22 is an SEM of a polyester support media and Figure 23 is the membrane pressurized on that surface. Note the impressions in the membrane which correspond with the physical appearance of the cloth support.

Similar observations can be made from the membrane pressurized in the porous fiber glass/epoxy tube without a liner (Figures 24 and 25). Such dimensional changes result in membrane orientation or drawing, occasionally resulting in loss of membrane selectivity.

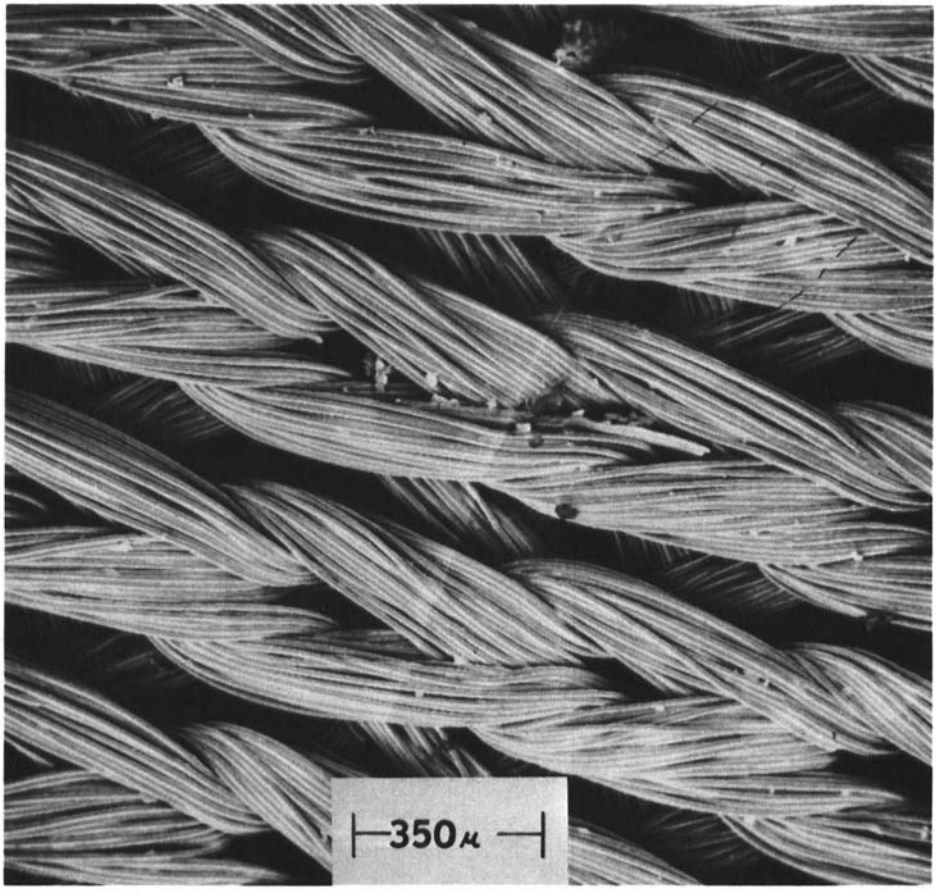

FIGURE 22
Scanning electron photomicrograph of a polyester support surface

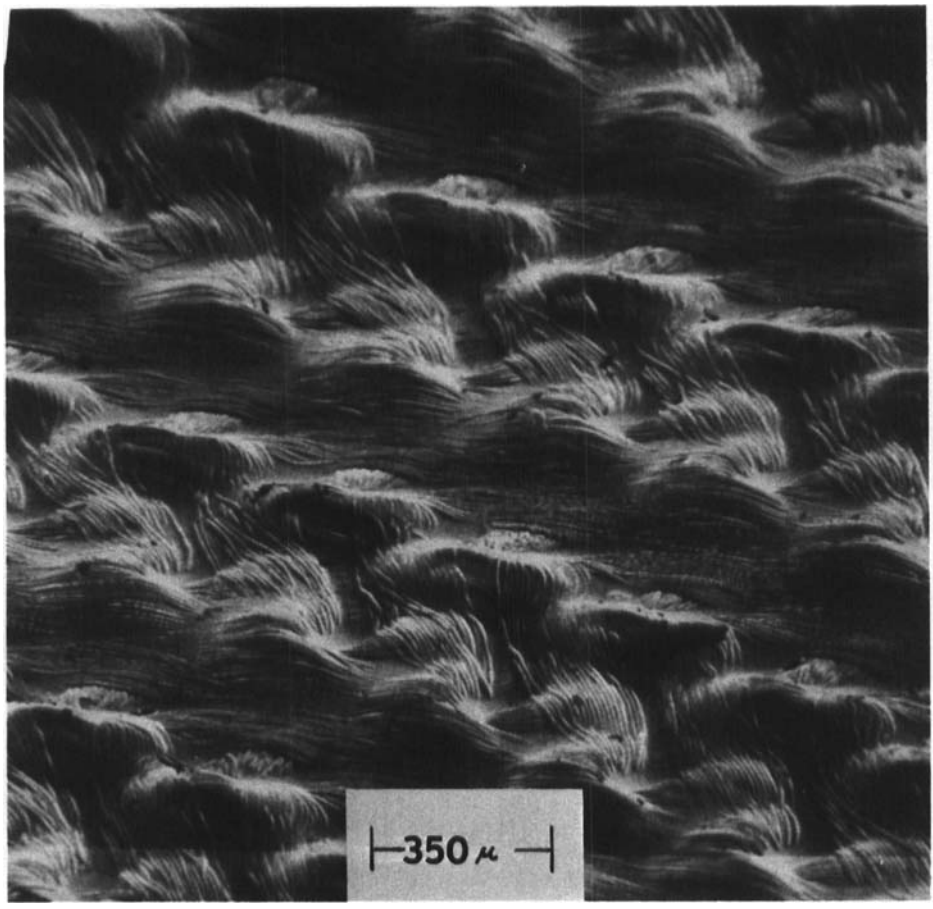

FIGURE 23
Scanning electron photomicrograph of a Polymer I tubular membrane surface pressured at 102 atms for 48 hours on the polyester support surface

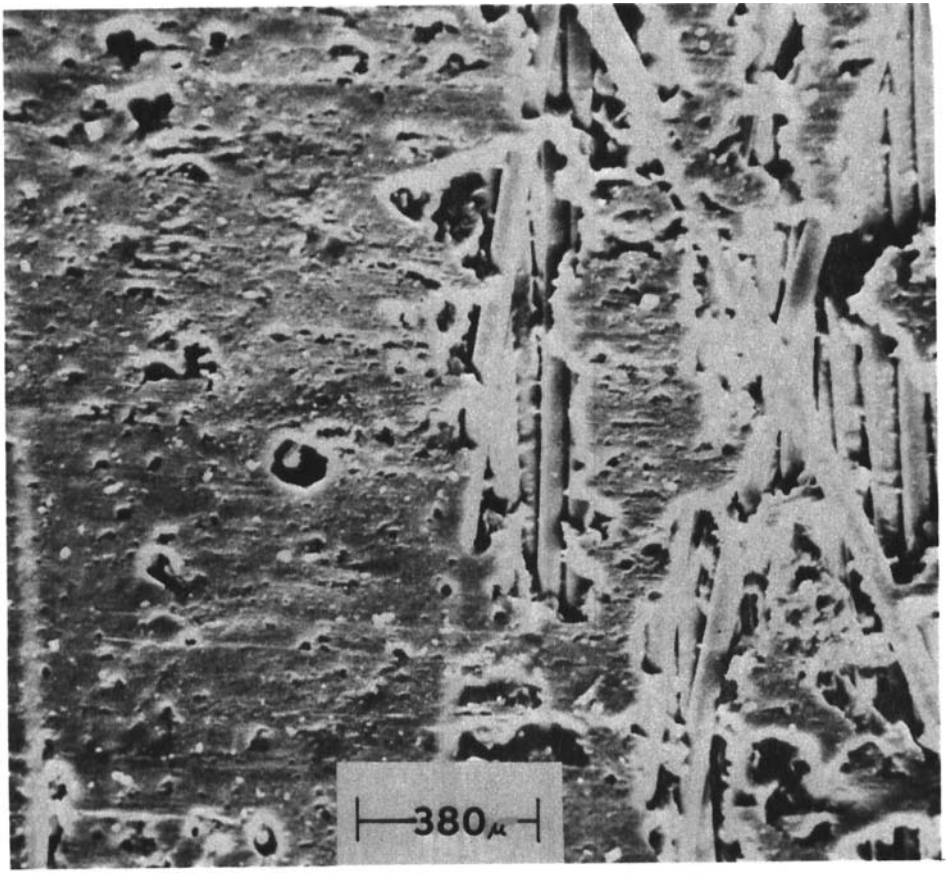

FIGURE 24
Scanning electron micrograph of the inside wall of the porous fiber glass/epoxy composite tube

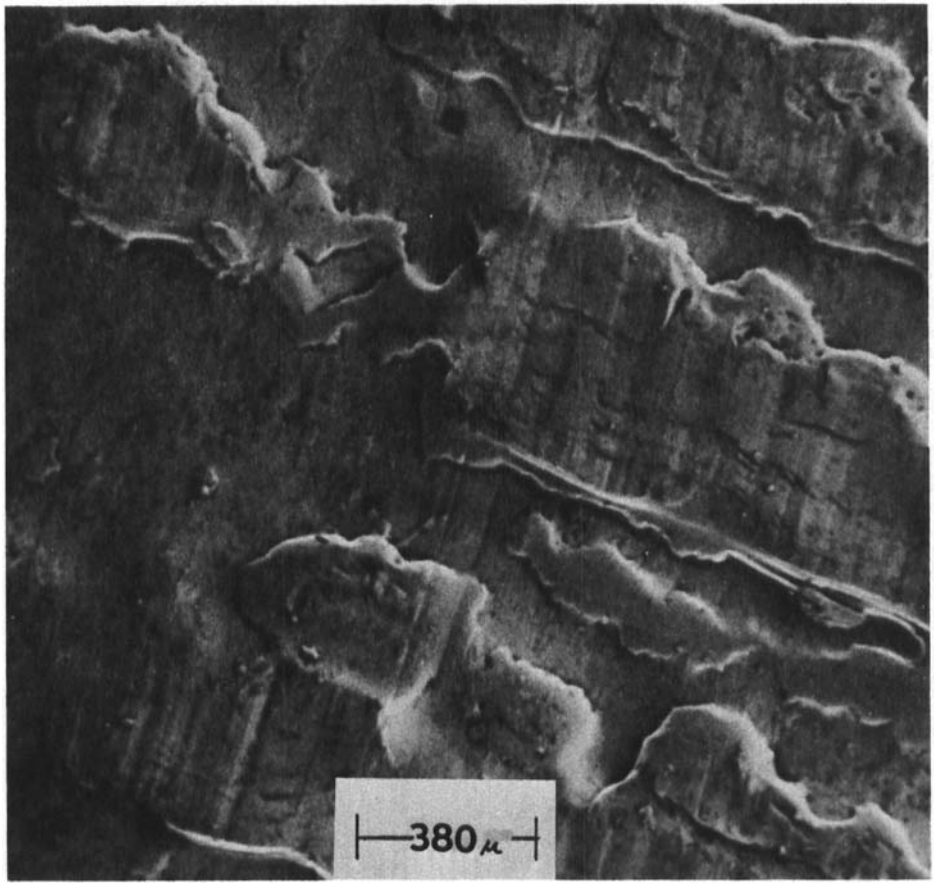

FIGURE 25

Scanning electron micrograph of a Polymer I tubular membrane surface pressurized at 102 atms for 48 hours directly on the fiber glass/epoxy porous composite tube

Comparative reverse osmosis performance, for the two previously discussed supports (composite tube with and without polyester liner), is summarized in Table XV. The higher flux decay rates, for the membrane supported on the polyester cloth, indicated a greater degree of membrane deformation under pressure. This is as would be expected from the observations made in Figures 23 and 25.

Typical reverse osmosis performance for tubular polyamide membranes is provided in Table XVI.

B. Hollow Fiber Membranes

The preparation of asymmetric hollow fibers, from solutions containing aromatic polyamides, follows a procedure analogous to that established for flat and tubular membrane formation: membrane casting, solvent evaporation and finally coagulation.

TABLE XV

Comparative Reverse Osmosis Data for Polymer I
Tubular Membranes with Selected Supports

Tubular Membrane Support Media	J_1 (g/cm^2-sec)	Flux Decay ($d \log J_1 / d \log t$)	r
direct tube	4.10×10^{-4}	-0.12	0.996
polyester cloth	4.25×10^{-4}	-0.24	0.992

Porous fiber glass/epoxy composite tube used in this experiment had an intrinsic flux (w/o membrane) of 1.7×10^{-2} g/cm^2-sec at 1.36 atms applied pressure.

TABLE XVI

Reverse Osmosis Performance for Selected Aromatic Polyamide Tubular Membranes

Polymer	J_1 (g/cm^2-sec)	r
I	4.1×10^{-4}	0.996
II	4.6×10^{-4}	0.994
IV	5.9×10^{-4}	0.991

Reverse osmosis data taken at 102 atms with a 0.60M NaCl test solution.

Hollow fiber "casting" was achieved by the extrusion of a highly viscous (ca. 10^5 poise) solution through one of the specially designed dies or spinnerettes shown in Figure 26. The tube-in-orifice type was most frequently used because it afforded greater latitude in controlling fiber diameters.

Typical solution compositions contained 16-20 g/dl of polymer in a dimethylacetamide-calcium chloride mixture. The high solution viscosity-solution concentration requirements were necessary to provide a stabilized tubular extrudate over the long drying intervals required for membrane skin development.

Solvent evaporation was carried out in a dry-spin tower at temperatures in the range: $100 \leq t, ^\circ C \leq 200$ as illustrated in Figure 27. By use of this thermostated column, solvent was evaporated from the emerging thread line and carried from the

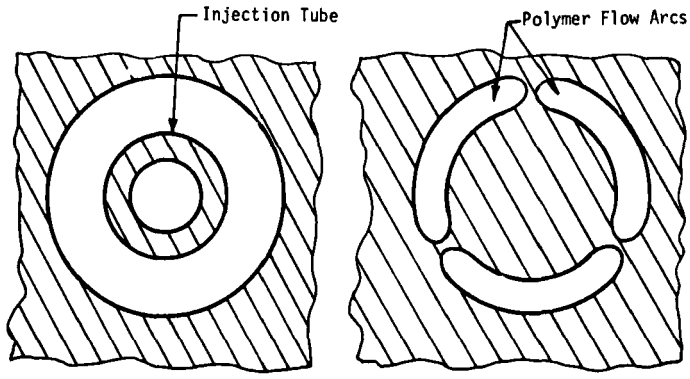

FIGURE 26
Hollow fiber spinnerettes

column by means of a nitrogen gas sweep. Fiber take up rates as high as 1000 cm/min were used with this system.

Fiber cross-sections, typical of the ones prepared by this procedure, are illustrated by the photomicrographs in Figures 28 and 29. Each photomicrograph shows fibers of reasonably uniform cross-sections.

Bundles of the dry-spun fibers were potted dry using an epoxy sealer, then tested in a reverse osmosis cell similar to the one shown in Figure 30.

Typical reverse osmosis performance for the dry-spun aromatic polyamide hollow fibers (Polymer I) is shown in Table XVII. The relatively low flux compared with flat films

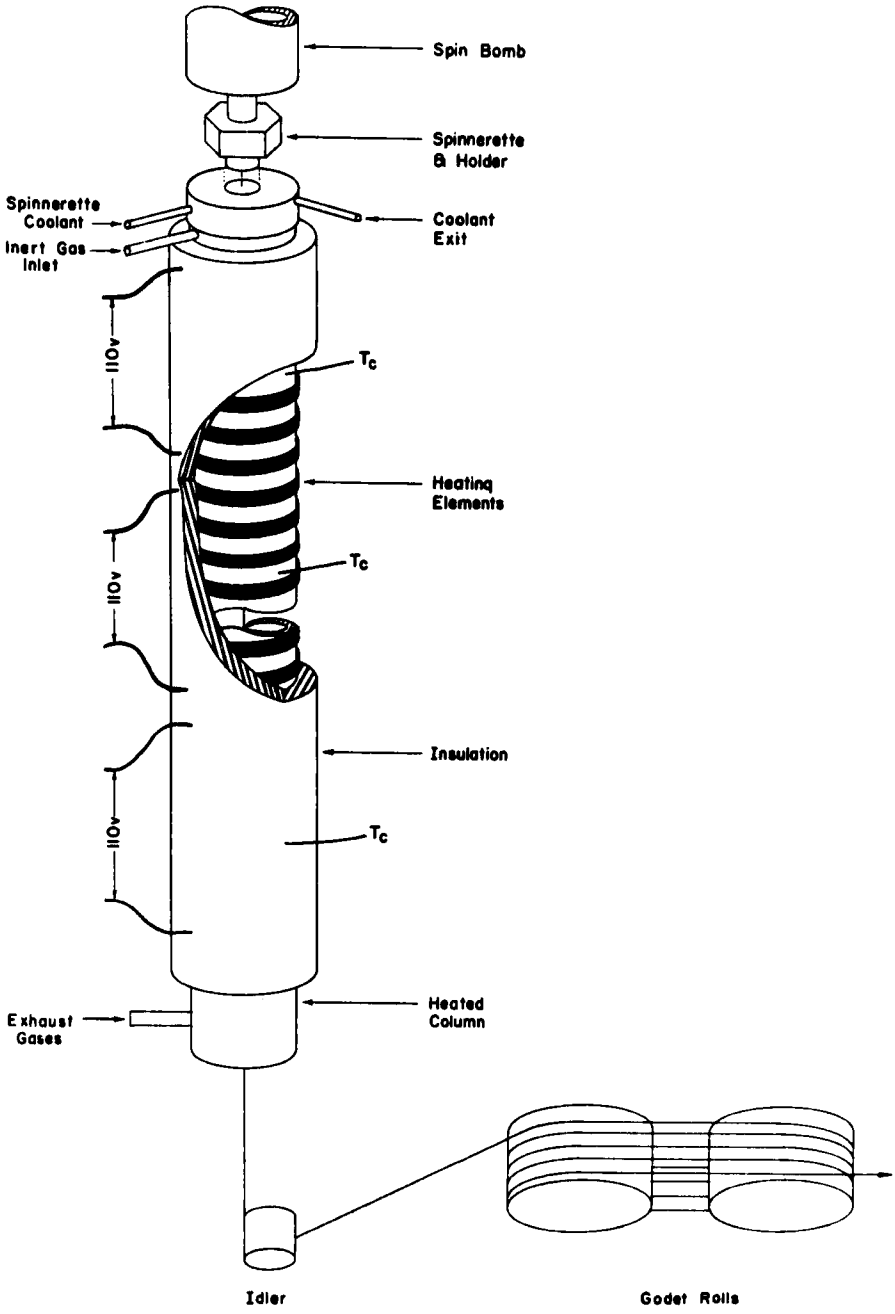

FIGURE 27
A diagram of a dry-spinning line for preparation of aromatic polyamide hollow fibers

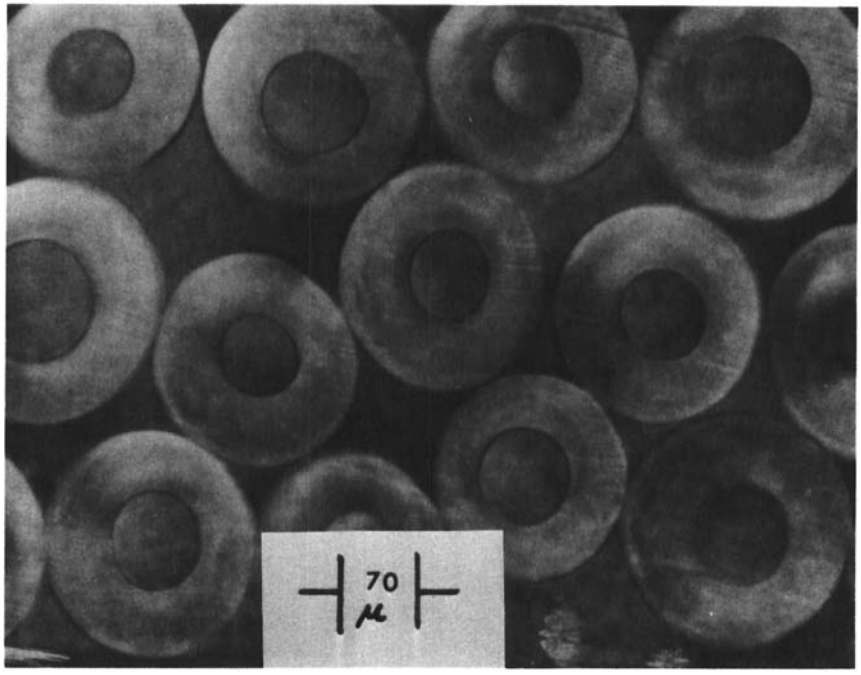

FIGURE 28
Photomicrograph of dry-spun Polymer I hollow fibers
(Sample A)

TABLE XVII

Typical Reverse Osmosis for Dry-spun Polymer I
Hollow Fibers

Fiber Sample	NaCl Test Solution (g/cm^3)	P (atms)	J_1 10^5 (g/cm^2-sec)	r	$10^7 \frac{J_1}{(\Delta P - \Delta \pi)}$ $\frac{(g\text{-atm}}{cm^2\text{-sec})}$
A	0.100	51	1.89	0.991	4.39
	0.207	68	1.51	0.992	2.92
	0.362	68	1.13	0.994	2.76
B	0.365	68	0.04	0.996	0.10

Reverse osmosis data taken at 24° C.

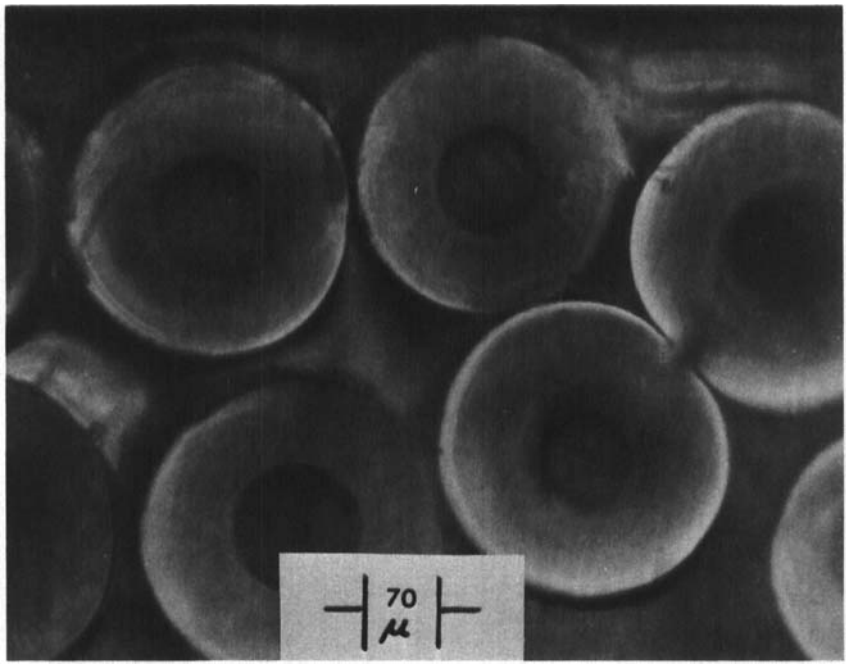

FIGURE 29
Photomicrograph of dry-spun Polymer I hollow fibers
(Sample B)

and tubes suggest a rather thick skin, dense matrix, or both. It is the latter assumption that is verified by electron microscopy, as shown in Figures 31 through 34.

In Figure 31 a stabilized hollow fiber cross-section is seen with both outside and bore surfaces visible. An enlargement of the air-dried surface region (Figure 32) shows a highly consolidated matrix structure and a thick (ca. 0.4 micron), dense skin. An enlarged section of the fiber wall interior (Figure 33)

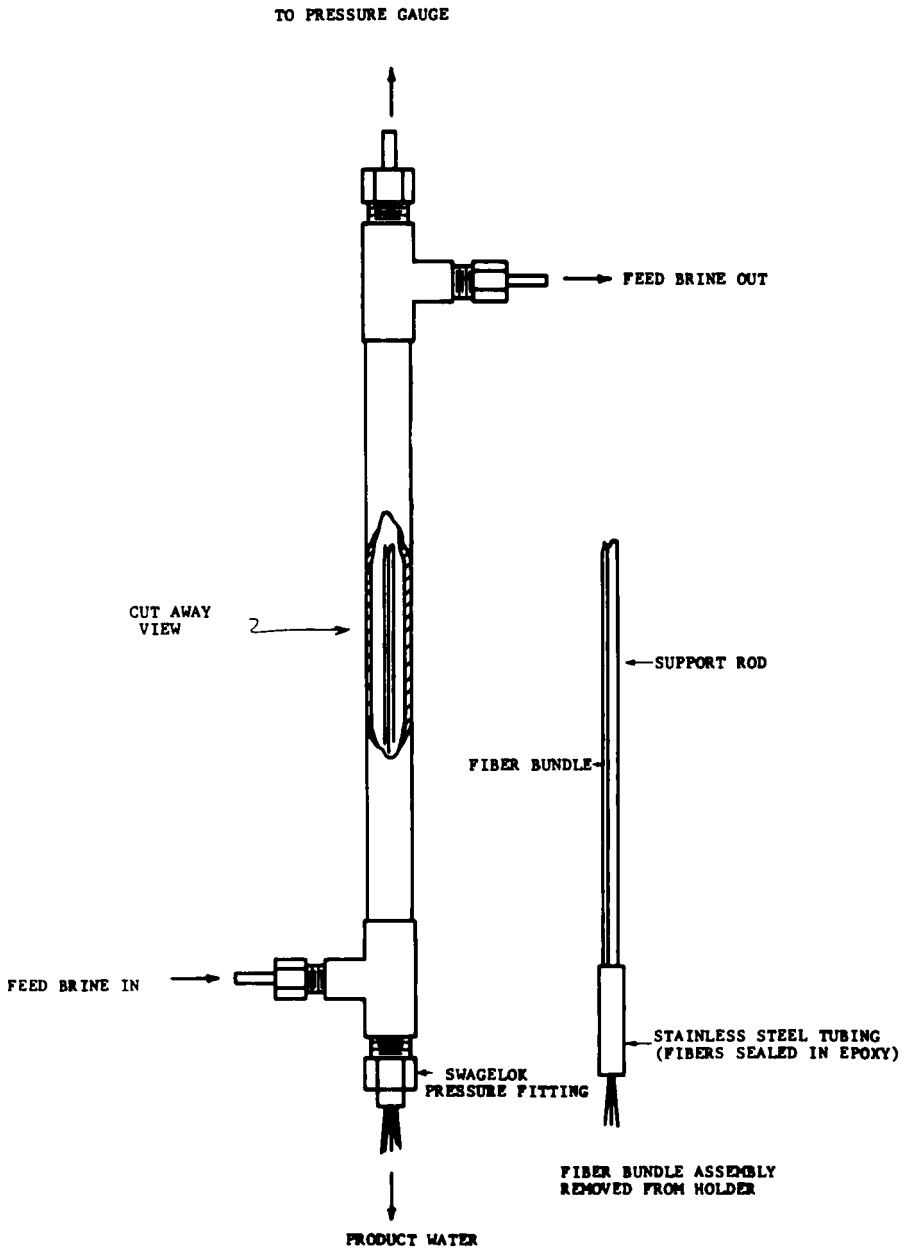

FIGURE 30
Hollow fiber reverse osmosis test cell

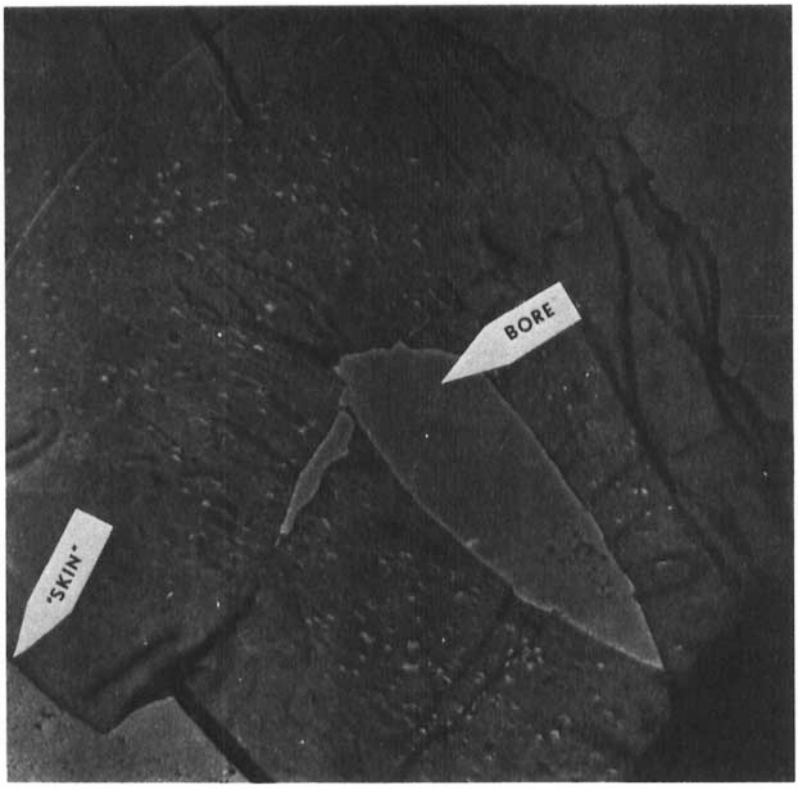

FIGURE 31
Electron photomicrograph of a Polymer I hollow fiber cross-section

shows some fine structural detail, including some very large voids. The surface area of the inner wall (bore) appears dense and not too dissimilar from that found with the flat films. Such cross-sectional structure appears to be the result of a rapid initial drying, which produces the thick skin, followed by very low coagulation rates at relatively high residual solvent levels.

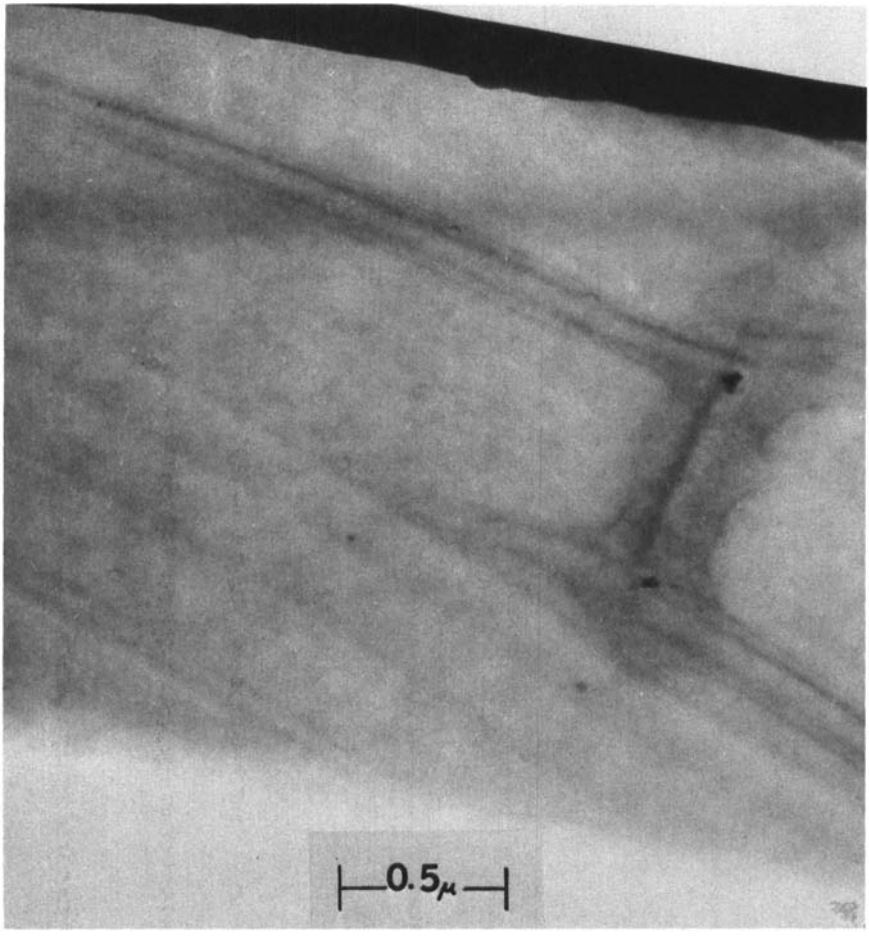

FIGURE 32
Electron photomicrograph of the air-dried surface region of a Polymer I hollow fiber

ACKNOWLEDGMENTS

The author wishes to acknowledge the contributions of Messrs. J. A. Carden, W. L. Hofferbert, L. C. Locust, M. C. Readling and J. H. Rhodes in carrying out the work

FIGURE 33
Electron photomicrograph of the interior region
of a Polymer I hollow fiber

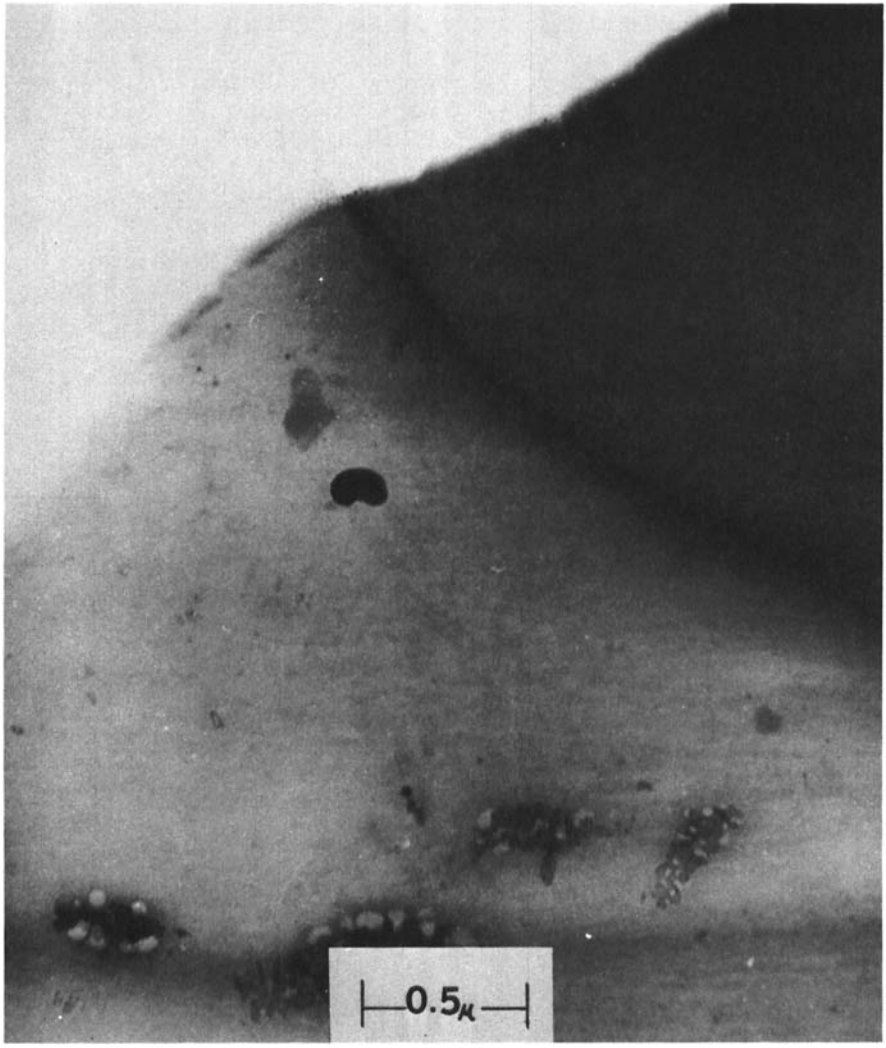

FIGURE 34
Electron photomicrograph of the inner wall (bore) region of a Polymer I hollow fiber

described. Additional thanks are due Dr. V. F. Holland of this laboratory for the electron microscopy; Dr. William Walsh of the School of Textiles, North Carolina State University, Raleigh, N. C. for providing the equipment used in the radiation experiments; Dr. H. W. Habgood, Chief of the Physical Sciences Branch, Research Council of Alberta, Edmonton, Alberta, Canada for his generosity in providing the gas transport data; Mrs. L. O. Hopson for secretarial assistance and Dr. T. A. Orofino for his many helpful suggestions during the preparation of this manuscript. Most of the work reported was carried out under Contract Numbers 14-01-0001-1720 and 14-30-2642, granted to Monsanto Research Corporation by the Membrane Division, Office of Saline Water, U. S. Department of the Interior.

REFERENCES

1. C. E. Reid and E. J. Breton, Jr., J. Appl. Poly. Sci., 1, 133 (1959).

2. S. Loeb and S. Sourirajan, "Sea Water Demineralization by Means of a Semipermeable Membrane," UCLA Report No. 60-60, July 1960.

3. S. Loeb and F. Milstein, DECHEMA (Deut. Ges. Chem. Apparatewesen Monogr.), 47, 805 (1962).

4. T. A. Orofino et al., "Development of Hollow Filament Technology for Reverse Osmosis Desalination Systems," OSW Research and Development Progress Report No. 549, May 1970.

5. R. McKinney, Jr., Polymer Preprints, 12, 365, Sept. 1971.

6. R. McKinney, Jr. and J. H. Rhodes, Macromol., 4, 633 (1971).

7. J. W. Richter and H. H. Hoehn, U. S. Patent 3,567,632 (1971).

8. C. M. Hansen, J. Oil & Col. Chem. Assoc., 51, 1 (1968).

9. C. M. Hansen, Ind. Eng. Chem. Prod. Rec. Develop., 8, 282 (1970).

10. R. McKinney, Jr., Anal. Chem., 41, 1513 (1969).

11. U. Merten, "Desalination by Reverse Osmosis," MIT Press, Cambridge, 1966.

12. E. S. Perry and C. J. Van Oss, "Progress in Separation and Purification," 3, Wiley, New York, 1970.

13. A. S. Michaels, in "Proceedings of the Symposium on Membrane Processes for Industry," Southern Research Institute, Birmingham, May, 1966.

14. H. W. Habgood, Research Council of Alberta, Edmonton, Alberta, Canada, private communication.

15. C. J. Gittens et al., Desalination, 8, 369 (1970).

16. M. A. Frommer, Hydronautics, Inc., Laurel, Maryland private communication.

17. R. McKinney, Jr. et al., "Development of Polyamide Reverse Osmosis Membranes for Seawater Desalination," OSW Research and Development Progress Report, in press.

18. S. Loeb, Desalination, 1, 1 (1966).